


NQR and NMR spectra in the odd-parity multipole material CeCoSi

Megumi Yatsushiro^{1,2} and Satoru Hayami²

¹*Department of Physics, Hokkaido University, Sapporo 060-0810, Japan*

²*Department of Applied Physics, The University of Tokyo, Tokyo 113-8656, Japan*

 (Received 3 August 2020; revised 30 October 2020; accepted 11 November 2020; published 30 November 2020)

We study theoretically NQR and NMR spectra in the presence of odd-parity multipoles originating from staggered antiferromagnetic and antiferroquadrupole orderings. For the f -electron metal CeCoSi, which is a candidate hosting odd-parity multipoles, we derive an effective hyperfine field acting on a Co nucleus generated from electronic origin multipole moments of the Ce ion in zero and nonzero magnetic fields. We elucidate that emergent odd-parity multipoles give rise to sublattice-dependent spectral splittings in NQR and NMR through the effective hyperfine coupling in the absence of global inversion symmetry. We mainly examine the behaviors of the NQR and NMR spectra in three odd-parity multipole ordered states: a y -type magnetic toroidal dipole order with a staggered x -type antiferromagnetic structure, an xy -type electric toroidal quadrupole order with a staggered $(x^2 - y^2)$ -type antiferroquadrupole structure, and a z -type electric dipole order with a staggered $(3z^2 - r^2)$ -type antiferroquadrupole structure. We show that different odd-parity multipole orders lead to different field-dependent spectral splittings in NMR, while only the xy -type electric toroidal quadrupole order exhibits the NQR spectral splitting. We also present possible sublattice-dependent spectral splittings for all the odd-parity multipole orders potentially activated in low-energy crystal-field levels, which will be useful to identify odd-parity order parameters in CeCoSi by NQR and NMR measurements.

DOI: [10.1103/PhysRevB.102.195147](https://doi.org/10.1103/PhysRevB.102.195147)

I. INTRODUCTION

Spatial inversion symmetry is one of the fundamental symmetries in solids. In recent studies, spontaneous inversion symmetry breaking by electronic orderings has attracted much attention, as it leads to fascinating phenomena, such as magnetoelectric effect [1–3] and nonreciprocal transport properties [4]. Once the systems undergo phase transitions causing inversion symmetry breaking, order parameters are represented by unconventional odd-parity multipoles, such as magnetic toroidal dipoles [5–9], magnetic quadrupoles [10–12], electric toroidal quadrupoles [13,14], and electric octupoles [15–17]. In previous studies, such odd-parity multipoles have often been described by the staggered (antiferroic) alignment of even-parity multipoles on a crystal structure without local inversion symmetry at an atomic site; prototypes are the zigzag chain [7,18], honeycomb structure [6,8], and diamond structure [19,20]. Such odd-parity multipoles formed by an antiferroic alignment of even-parity multipoles like magnetic dipoles and electric quadrupoles are referred to as cluster odd-parity multipoles.

Meanwhile, it is still an open issue how to detect cluster odd-parity multipoles. As emergent odd-parity multipoles are a source of physical phenomena related to inversion symmetry breaking as mentioned above, the presence/absence of odd-parity multipoles can be distinguishable through macroscopic measurements. However, it is difficult to obtain microscopic information with respect to odd-parity multipoles from those measurements because measured physical quantities are sensitively affected by various factors such as domain distributions and electronic band structures. Thus, the use

of probes, such as second harmonic generation [21,22] and magnetoelectric optics [23–31], to directly detect odd-parity multipoles is promising. For example, the second harmonic generation enables us to detect the domain structure of odd-parity magnetic quadrupoles and magnetic toroidal dipoles and the resonant magnetoelectric x-ray scattering provides the temperature dependence of the odd-parity magnetic toroidal dipole moment.

The NQR and NMR measurements are also sensitive microscopic probes used to detect electronic multipoles through nuclear spins, which have been developed for exploring atomic-scale electric quadrupoles and magnetic dipoles/octupoles in localized f -electron materials such as $Ce_{1-x}La_xB_6$ [32–44], NpO_2 [44–46], and skutterudite RT_4X_{12} (R denotes a rare earth, T a transition metal, and X a pnictogen) [47–50]. However, the studies using NQR and NMR measurements have been limited to even-parity multipoles with respect to the spatial inversion operation, as nuclear spins and their products are characterized as even-parity tensors.

In the present study we propose that NQR and NMR can be good probes used to detect cluster odd-parity multipoles. To demonstrate that, we analyze NQR and NMR spectra under the odd-parity multipole orderings by considering the candidate CeCoSi, which may host two types of odd-parity multipole orders depending on temperature and pressure [51–58]. The crystal structure of CeCoSi is the centrosymmetric CeFeSi-type structure ($P4/nmm$, D_{4h}^7 , No. 129) in Fig. 1(a), where there is no inversion center on each atom; Ce and Si have C_{4v} symmetry and Co has D_{2d} symmetry [59]. Such a crystal structure without local inversion symmetry at an atomic site enhances the chance to realize the cluster odd-

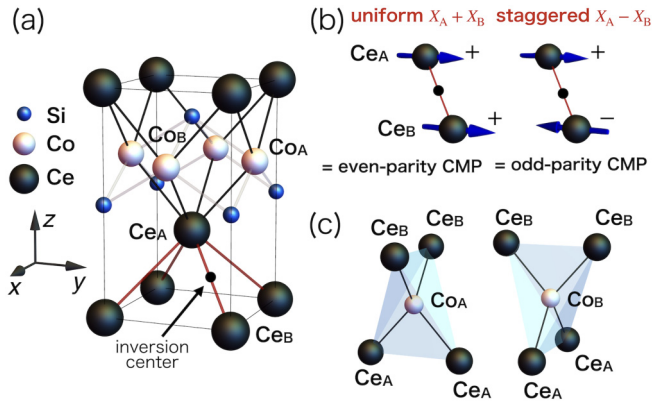


FIG. 1. (a) Tetragonal crystal structure of CeCoSi. The nearest-neighbor Ce-Ce, Ce-Co, and Co-Si bonds are represented by red, black, and gray solid lines, respectively. The rectangle represents a unit cell. (b) Uniform and staggered alignments of local even-parity multipoles in a unit cell, $X_A + X_B$ and $X_A - X_B$, which correspond to cluster even-parity and odd-parity multipoles (CMP) $X^{(c)}$, respectively. As an example, uniform and staggered alignments of M_y are shown. (c) Ce tetrahedrons surrounding Co_A (left) and Co_B (right) sites.

parity multipoles by the antiferroic alignment of even-parity multipoles as mentioned above. In this compound, as two different Ce sites Ce_A and Ce_B are located at positions without local inversion symmetry and the inversion center is present at their bond center, the staggered even-parity multipole order at those Ce sites breaks the global inversion symmetry, which corresponds to the emergence of odd-parity multipole orders [60,61]. Recently, the antiferromagnetic (AFM) ordered state at low temperature was identified as a staggered alignment of the magnetic moments along the [100] direction with the ordering vector $\mathbf{q} = \mathbf{0}$ by the neutron diffraction measurement [56], whereas the other phase mainly found under pressure [referred to as the pressure-induced ordered phase (PIOP)] might correspond to the antiferroquadrupole (AFQ) phase, although it is an as-yet unidentified phase [53,54]. Theoretically, the authors clarified that odd-parity multipole moments are induced when the staggered AFM and AFQ phases are realized [60]: The identified AFM state corresponds to the cluster magnetic toroidal dipole order and the AFQ state corresponds to any of the cluster electric toroidal quadrupole or cluster electric dipole orders depending on the types of electric quadrupoles of the Ce ion. Thus, CeCoSi is expected to exhibit electronic-order-driven noncentrosymmetric physics, such as the Edelstein effect, magnetoelectric effect, and current-induced piezoelectric effect, which originate from the cluster odd-parity multipoles [60].

For observed or suggested odd-parity multipole orderings, we derive a general form of the hyperfine field on the ^{59}Co nucleus at zero and nonzero magnetic fields with the aid of magnetic point group analysis. We elucidate that the Co nuclear spins are coupled with the odd-parity order parameters from Ce ions once the spatial inversion symmetry is broken by spontaneous even-parity multipole orderings. The hyperfine couplings arising from the odd-parity multipoles induce the sublattice-dependent NQR and NMR spectral splittings. We show that different odd-parity multipole orders give rise to

different field-dependent NMR spectral splittings, e.g., the y -type magnetic toroidal dipole in the x -type AFM structure shows sublattice-dependent splitting except for the magnetic field normal to the [010] direction. Furthermore, we find that only the xy -type electric toroidal quadrupole order arising from the $(x^2 - y^2)$ -type AFQ structure induces sublattice-dependent NQR spectral splitting. We also show that the hyperfine fields from the odd-parity multipoles can be evaluated from NQR and NMR splittings. Our result indicates that the NQR and NMR spectra in noncentrosymmetric systems will not only provide information of microscopic hyperfine fields regarding odd-parity multipoles but also be useful in identifying what types of odd-parity multipoles emerge.

This paper is organized as follows. In Sec. II we introduce the multipole degrees of freedom and the local Hamiltonian of Ce ions. In Sec. III the effective hyperfine field acting on the Co nucleus is derived based on the symmetry discussion. The NQR and NMR spectra in the odd-parity multipole orders are shown in Secs. IV and V, respectively. We summarize the NQR and NMR splittings for possible odd-parity order parameters in Sec. VI. Section VII summarizes this paper. We discuss the molecular mean-field dependence of the odd-parity multipole moments in Appendix A, show the spectra of the field-swept NMR in Appendix B, present the result of the [110]-field NMR in Appendix C, and summarize the result for another choice of crystal-field level in Appendix D.

II. LOCAL MULTIPOLE MOMENT OF THE Ce ION

We introduce electronic multipole degrees of freedom of Ce ions in this section. We present the local multipole degrees of freedom in a $4f$ electron of the Ce ion in Sec. II A, we construct the local Hamiltonian in Sec. II B, and we show the behavior of the multipole moments induced by the AFM and AFQ states in Sec. II C.

A. Multipole degrees of freedom

We briefly review the local and cluster multipole degrees of freedom in CeCoSi following Ref. [60]. We take into account multipoles activated in the $J = 5/2$ multiplet from the f^1 configuration in a Ce^{3+} ion. The sixfold degeneracy of the $J = 5/2$ multiplet splits into one Γ_6 level and two Γ_7 levels in the tetragonal crystal field. The experiments indicate that the first- and second-excited states are located above 100 and 150 K, respectively, from the ground state [54,56]. In the present discussion, we consider the local multipole degrees of freedom of a Ce ion described by the low-energy crystal-field levels up to the first-excited level. We assume that the low-energy levels consist of the ground-state Γ_7 doublet and the first-excited Γ_6 doublet in C_{4v} site symmetry [60]. Within these low-energy levels, even-parity electric and magnetic multipoles with rank $l \leq 5$ are activated, as discussed below [60,62–65]. We also show the result for other low-energy levels, which consist of two Γ_7 doublets, in Appendix D.

For the basis function $\phi = (\phi_{\Gamma_6\uparrow}, \phi_{\Gamma_6\downarrow}, \phi_{\Gamma_7\uparrow}, \phi_{\Gamma_7\downarrow})$, where \uparrow, \downarrow represent the quasispins, the local multipole degrees of freedom of the Ce ion are expressed as the tensor product of two Pauli matrices σ_μ within the Γ_6 or Γ_7 doublet and τ_μ between the Γ_6 - Γ_7 doublets for $\mu = 0, x, y, z$ (σ_0 and τ_0 are

unit matrices) [66]. All 16 multipoles are given as follows: an electric monopole (charge) $\hat{Q}_0 = \frac{1}{2}\sigma_0\tau_0$; two sets of three magnetic dipoles $(\hat{M}_x^\Gamma, \hat{M}_y^\Gamma, \hat{M}_z^\Gamma) = \frac{1}{4}(\sigma_x, \sigma_y, \sigma_z)(\tau_0 \pm \tau_z)$, where the sign is + (−) for the $\Gamma = \Gamma_6$ (Γ_7) level; and an electric quadrupole $\hat{Q}_u (=3z^2-r^2) = \frac{1}{2}\sigma_0\tau_z$ in a Hilbert space within the Γ_6 or Γ_7 doublet; and two magnetic dipoles $(\hat{M}'_x, \hat{M}'_y) = \frac{1}{2}(\sigma_x\tau_x, -\sigma_y\tau_x)$, four electric quadrupoles $(\hat{Q}_v (=x^2-y^2), \hat{Q}_{xy}, \hat{Q}_{yz}, \hat{Q}_{zx}) = \frac{1}{2}(\sigma_0\tau_x, \sigma_z\tau_y, \sigma_x\tau_y, \sigma_y\tau_y)$, and two magnetic octupoles $(\hat{M}_{xyz}, \hat{M}_z^\beta) = \frac{1}{2}(\sigma_0\tau_y, \sigma_z\tau_x)$ activated in a Hilbert space between the Γ_6 - Γ_7 doublets.

As there are two Ce ions in a unit cell, Ce_A and Ce_B, as shown in Fig. 1(a), order parameters without breaking the translational symmetry are described by the uniform or staggered component of multipole moments in Ce_A and Ce_B sites: the uniform component $\hat{X}_A + \hat{X}_B$ and staggered component $\hat{X}_A - \hat{X}_B$, where \hat{X}_i stands for the above multipole degrees of freedom at site $i = A, B$. In terms of symmetry, uniform and staggered components are assigned as either cluster even- or odd-parity multipoles, as shown in Fig. 1(b) [60]. We adopt the lowest-rank multipoles from the four types of multipole expressions (electric, magnetic, electric toroidal, and magnetic toroidal) in each uniform and staggered order [67,68], as the multipoles with a different rank belong to the same irreducible representation in a lattice system. For the uniform component $\hat{X}_A + \hat{X}_B$, cluster even-parity multipoles are defined as an electric monopole $\hat{Q}_0^{(c)}$ when the local multipole X is \hat{Q}_0 , three magnetic dipoles $(\hat{M}_x^{(c)}, \hat{M}_y^{(c)}, \hat{M}_z^{(c)})$ when X is $\sum_\Gamma(\hat{M}_x^\Gamma, \hat{M}_y^\Gamma, \hat{M}_z^\Gamma) + (\hat{M}'_x, \hat{M}'_y, 0)$ ($\Gamma = \Gamma_6, \Gamma_7$) [69], five electric quadrupoles $(\hat{Q}_u^{(c)}, \hat{Q}_v^{(c)}, \hat{Q}_{yz}^{(c)}, \hat{Q}_{zx}^{(c)}, \hat{Q}_{xy}^{(c)})$ when X is $(\hat{Q}_u, \hat{Q}_v, \hat{Q}_{yz}, \hat{Q}_{zx}, \hat{Q}_{xy})$, and two magnetic octupoles $(\hat{M}_{xyz}^{(c)}, \hat{M}_z^{\beta(c)})$ when X is $(\hat{M}_{xyz}, \hat{M}_z^\beta)$. Meanwhile, since the staggered component $\hat{X}_A - \hat{X}_B$ shows odd parity with respect to the spatial inversion operation, the cluster odd-parity multipoles are defined by the staggered component as electric dipoles $(\hat{Q}_x^{(c)}, \hat{Q}_y^{(c)}, \hat{Q}_z^{(c)})$ when X is $(\hat{Q}_{zx}, \hat{Q}_{yz}, \hat{Q}_0 + \hat{Q}_u)$ [70], magnetic toroidal dipoles $(\hat{T}_y^{(c)}, -\hat{T}_x^{(c)})$ when X is $\sum_\Gamma(\hat{M}_x^\Gamma, \hat{M}_y^\Gamma) + (\hat{M}'_x, \hat{M}'_y)$ [69], electric toroidal quadrupoles $(\hat{G}_{xy}^{(c)}, \hat{G}_v^{(c)})$ when X is $(\hat{Q}_v, \hat{Q}_{xy})$, and magnetic quadrupoles $(\hat{M}_u^{(c)}, \hat{M}_{xy}^{(c)}, \hat{M}_v^{(c)})$ when X is $(\sum_\Gamma \hat{M}_z^\Gamma, \hat{M}_{xyz}, \hat{M}_z^\beta)$ [69]. For clarity, we introduce the superscript (c) as the denotation for cluster multipoles. The correspondence of local and cluster multipoles is summarized in Table I. Hereafter, we use the denotation of the cluster multipoles $\hat{X}^{(c)}$ instead of $\hat{X}_A + \hat{X}_B$ and $\hat{X}_A - \hat{X}_B$ to clearly represent the effect of the odd-parity multipoles on NQR and NMR spectra.

B. Local Hamiltonian for 4f electrons

To examine a hyperfine field on the ⁵⁹Co nucleus, we need to take into account an effective field generated from the Ce site. As described below, an effective hyperfine field on the ⁵⁹Co nucleus depends on the types of multipole orderings of 4f electrons at the Ce site. We here introduce a local Hamiltonian for the Ce electron at the phenomenological level to incorporate the effect of odd-parity multipoles. The local

TABLE I. Correspondence of (a) uniform $\hat{X}_A + \hat{X}_B$ components to cluster even-parity multipoles and (b) staggered $\hat{X}_A - \hat{X}_B$ components to cluster odd-parity multipoles. Magnetic dipoles $(\hat{M}_x^{\text{tot}}, \hat{M}_y^{\text{tot}}, \hat{M}_z^{\text{tot}})$ represent $\hat{M}_\mu^{\text{tot}} = \sum_\Gamma \hat{M}_\mu^\Gamma + \hat{M}'_\mu$ for $\mu = x, y$ and $\hat{M}_z^{\text{tot}} = \sum_\Gamma \hat{M}_z^\Gamma$, where $\Gamma = \Gamma_6, \Gamma_7$ [69]. In the notation of the types of multipoles (MP), E, M, ET, and MT represent electric, magnetic, electric toroidal, and magnetic toroidal, respectively.

Cluster multipole	Type MP
(a) Uniform component	
$\hat{Q}_{0,A} + \hat{Q}_{0,B}$	$\hat{Q}_0^{(c)}$ E monopole
$\hat{M}_{x,A}^{\text{tot}} + \hat{M}_{x,B}^{\text{tot}}$	$\hat{M}_x^{(c)}$ x-type M dipole
$\hat{M}_{y,A}^{\text{tot}} + \hat{M}_{y,B}^{\text{tot}}$	$\hat{M}_y^{(c)}$ y-type M dipole
$\hat{M}_{z,A}^{\text{tot}} + \hat{M}_{z,B}^{\text{tot}}$	$\hat{M}_z^{(c)}$ z-type M dipole
$\hat{Q}_{u,A} + \hat{Q}_{u,B}$	$\hat{Q}_u^{(c)}$ $(3z^2 - r^2)$ -type E quadrupole
$\hat{Q}_{v,A} + \hat{Q}_{v,B}$	$\hat{Q}_v^{(c)}$ $(x^2 - y^2)$ -type E quadrupole
$\hat{Q}_{yz,A} + \hat{Q}_{yz,B}$	$\hat{Q}_{yz}^{(c)}$ yz-type E quadrupole
$\hat{Q}_{zx,A} + \hat{Q}_{zx,B}$	$\hat{Q}_{zx}^{(c)}$ zx-type E quadrupole
$\hat{Q}_{xy,A} + \hat{Q}_{xy,B}$	$\hat{Q}_{xy}^{(c)}$ xy-type E quadrupole
$\hat{M}_{xyz,A} + \hat{M}_{xyz,B}$	$\hat{M}_{xyz}^{(c)}$ xyz-type M octupole
$\hat{M}_{z,A}^\beta + \hat{M}_{z,B}^\beta$	$\hat{M}_z^{\beta(c)}$ $z(x^2 - y^2)$ -type M octupole
(b) Staggered component	
$\hat{Q}_{0,A} - \hat{Q}_{0,B}$	$\hat{Q}_z^{(c)}$ z-type E dipole
$\hat{M}_{x,A}^{\text{tot}} - \hat{M}_{x,B}^{\text{tot}}$	$\hat{T}_y^{(c)}$ y-type MT dipole
$\hat{M}_{y,A}^{\text{tot}} - \hat{M}_{y,B}^{\text{tot}}$	$-\hat{T}_x^{(c)}$ x-type MT dipole
$\hat{M}_{z,A}^{\text{tot}} - \hat{M}_{z,B}^{\text{tot}}$	$\hat{M}_u^{(c)}$ $(3z^2 - r^2)$ -type M quadrupole
$\hat{Q}_{u,A} - \hat{Q}_{u,B}$	$\hat{Q}_z^{(c)}$ z-type E dipole
$\hat{Q}_{v,A} - \hat{Q}_{v,B}$	$\hat{G}_{xy}^{(c)}$ xy-type ET quadrupole
$\hat{Q}_{yz,A} - \hat{Q}_{yz,B}$	$\hat{Q}_y^{(c)}$ y-type E dipole
$\hat{Q}_{zx,A} - \hat{Q}_{zx,B}$	$\hat{Q}_x^{(c)}$ x-type E dipole
$\hat{Q}_{xy,A} - \hat{Q}_{xy,B}$	$\hat{G}_v^{(c)}$ $(x^2 - y^2)$ -type ET quadrupole
$\hat{M}_{xyz,A} - \hat{M}_{xyz,B}$	$\hat{M}_{xy}^{(c)}$ xy-type M quadrupole
$\hat{M}_{z,A}^\beta - \hat{M}_{z,B}^\beta$	$\hat{M}_v^{(c)}$ $(x^2 - y^2)$ -type M quadrupole

Hamiltonian for sublattice i is given by

$$\mathcal{H}_{\text{Ce}_i} = \Delta(\hat{Q}_{0i} + \hat{Q}_{ui}) - \mathbf{H}^{(\text{el})} \cdot \hat{\mathbf{M}}_i \mp \sum_X h_X^s \hat{X}_i, \quad (1)$$

where Δ in the first term is the crystal-field energy of the Γ_6 level measured from the Γ_7 level ($\Delta > 0$), which is estimated as ~ 100 K [53]. We set $\Delta = 0.5$ in the following calculation. The second term in Eq. (1) is the Zeeman term for $\mathbf{H}^{(\text{el})} \equiv \mu_B \mathbf{H}$ coupled with the magnetic dipoles $\mathbf{M} = (M_x, M_y, M_z)$, where μ_B and \mathbf{H} are the Bohr magneton and magnetic field, respectively. We take the linear combination of the intraorbital components $\hat{M}_\mu^{\Gamma_6}$ and $\hat{M}_\mu^{\Gamma_7}$ and the interorbital component \hat{M}'_μ as $\hat{M}_\mu \equiv (\hat{M}_\mu^{\Gamma_7} + \delta^{\Gamma_6} \hat{M}_\mu^{\Gamma_6} \pm \delta' \hat{M}'_\mu)$ [the sign is + (−) for $\mu = x$ (y)] and $\hat{M}_z \equiv (\hat{M}_z^{\Gamma_7} + \delta^{\Gamma_6} \hat{M}_z^{\Gamma_6})$. The parameters δ^{Γ_6} and δ' are introduced to represent the difference of the magnetic susceptibility per different orbitals and are taken to be $(\delta^{\Gamma_6}, \delta') = (1/4, 1/2)$, which depend on the spin-orbit coupling and the crystal field [71]. The last term in Eq. (1) represents the multipolar mean fields leading to the multipole orderings with $\langle \hat{X}_i \rangle \neq 0$, which mimic the effect of

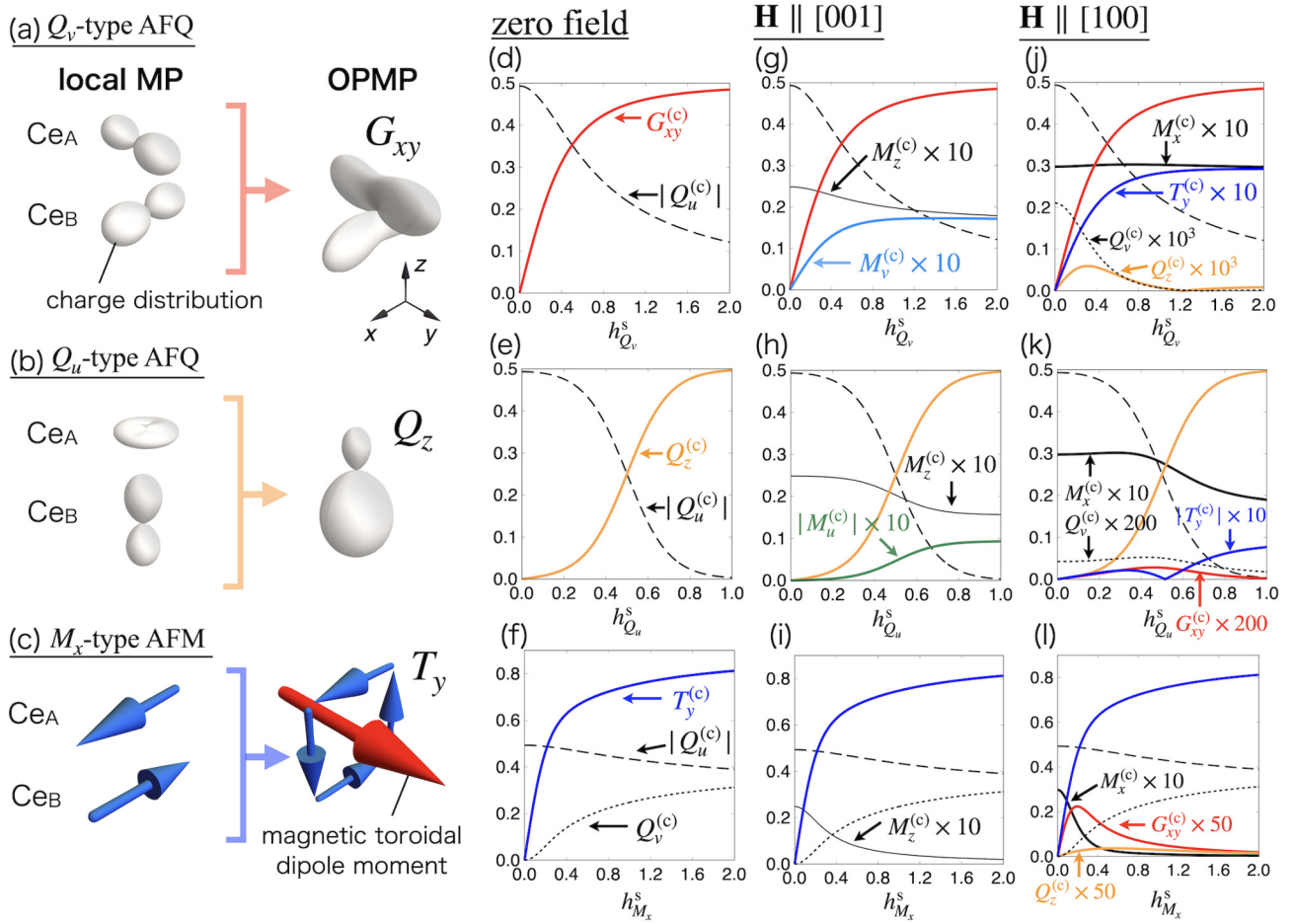


FIG. 2. (a)–(c) Schematics of local multipoles (MP) and cluster odd-parity multipoles (OPMP) in the (a) Q_v -type AFQ, (b) Q_u -type AFQ, and (c) M_x -type AFM states. The shape of the picture in (a) and (b) represents the charge distribution. The blue and red arrows in (c) represent the magnetic dipole and magnetic toroidal dipole moments, respectively. (d)–(l) Staggered mean-field dependence of multipoles in the (d)–(f) zero magnetic field, (g)–(i) magnetic field $\mathbf{H} \parallel [001]$, and (j)–(l) $\mathbf{H} \parallel [100]$. The data represent those in (d), (g), and (j) Q_v -type AFQ, (e), (h), and (k) Q_u -type AFQ, and (f), (i), and (l) M_x -type AFM states. Black solid and dashed lines represent the even-parity multipole moments, whereas colored solid lines are odd-parity multipole moments.

the Coulomb interaction. They originate from the mean-field decoupling for the intraorbital and interorbital Coulomb interaction terms [64]; the multipoles activated in a Γ_6 or Γ_7 level are relevant to the intraorbital Coulomb interaction, while those activated between the Γ_6 and Γ_7 levels are relevant to the interorbital Coulomb interaction. As we focus on the cluster multipoles induced by the staggered electronic orderings, we adopt the negative (positive) sign for the A (B) sublattice. For simplicity, we omit the multipole-multipole interaction between A and B sublattices, which is renormalized into h_{χ}^s at the mean-field level.

In the following discussion, we mainly consider three types of staggered orderings: M_x -type AFM, Q_u -type AFQ, and Q_v -type AFQ states, whose schematics are shown in Figs. 2(a)–2(c), respectively. This is because the neutron diffraction has indicated the M_x -type AFM state at low temperatures [56]. On the other hand, as the PIOP is still controversial, we discuss two types of AFQ states for candidates. One is the Q_u -type AFQ state arising from the intraorbital multipole degrees of freedom, while the other is the Q_v -type AFQ state arising from the interorbital multipole degrees of

freedom. For completeness, we also investigate other antiferroic multipole ordered states and the results are summarized in Sec. VI.

C. Multipoles in AFQ and AFM orderings

We discuss the behavior of the electronic multipole moments induced by the staggered mean field with and without the external magnetic field. We evaluate the thermal expectation value of the multipole moments $X \equiv \langle \hat{X} \rangle = \sum_n \langle n | \hat{X} | n \rangle \exp(-\beta E_n) / Z$, where $|n\rangle$ ($n = 1-8$) is the eigenstate with energy E_n of the total Hamiltonian $\mathcal{H}_{\text{CeA}} + \mathcal{H}_{\text{CeB}}$ and Z is a partition function. We set the inverse temperature $\beta = 10$, which corresponds to $T/\Delta = 0.2$.

Figures 2(d)–2(f) show all the nonzero multipole moments at zero magnetic field as a function of the staggered fields $h_{Q_v}^s$, $h_{Q_u}^s$, and $h_{M_x}^s$, respectively. It should be noted that $Q_u^{(c)}$ becomes nonzero irrespective of the types of order parameters due to nonzero Δ in Eq. (1). When the mean fields h_{χ}^s turn on, the corresponding cluster odd-parity multipole moments $X^{(c)}$ become nonzero.

TABLE II. Multipole moments induced in the Q_v -type AFQ, Q_u -type AFQ, and M_x -type AFM ordered states as well as the paramagnetic (Para) state. For nonzero fields, additional multipoles induced by \mathbf{H} are shown.

\mathbf{H}	Para	Q_v -type AFQ	Q_u -type AFQ	M_x -type AFM
zero	$Q_u^{(c)}$	$G_{xy}^{(c)}$	$Q_z^{(c)}$	$T_y^{(c)}, Q_v^{(c)}$
\parallel [001]	$M_z^{(c)}$	$M_v^{(c)}$	$M_u^{(c)}$	
\parallel [100]	$M_x^{(c)}, Q_v^{(c)}$	$Q_z^{(c)}, T_y^{(c)}$	$G_{xy}^{(c)}, T_y^{(c)}$	$Q_z^{(c)}, G_{xy}^{(c)}$

The results in the Q_v - and Q_u -type AFQ ordered states are shown in Figs. 2(d) and 2(e), respectively. The odd-parity electric toroidal quadrupole $G_{xy}^{(c)}$ is induced in the Q_v -type AFQ ordering, while the odd-parity electric dipole $Q_z^{(c)}$ is induced in the Q_u -type AFQ ordering. The mean-field dependence of the odd-parity moments are different from each other: $G_{xy}^{(c)}$ roughly increases as a function of $h_{Q_v}^s$, whereas $Q_z^{(c)}$ increases as a function of $(h_{Q_u}^s)^3$ in the small h_X^s region. This is attributed to the nature of the odd-parity order parameters, which is understood from the perturbation expansion for large Δ , as detailed in Appendix A.

According to the development of $G_{xy}^{(c)}$ or $Q_z^{(c)}$, $Q_u^{(c)}$ is suppressed in both AFQ states in different ways. In the case of the Q_v -type AFQ ordered state, $Q_u^{(c)}$ is suppressed as $(h_{Q_v}^s)^2$, while in the Q_u -type AFQ state it is suppressed as $(h_{Q_u}^s)^4$. The different mean-field dependences of the multipole moments give different multipole-field dependences of the NQR and NMR frequency shifts, as discussed in Secs. IV and V.

Figure 2(f) shows the result in the M_x -type AFM state with the odd-parity magnetic toroidal dipole moment $T_y^{(c)}$. The mean-field dependence of $T_y^{(c)}$ is similar to that in the Q_v -type AFQ ordering in Fig. 2(d). As a different point, the additional even-parity electric quadrupole $Q_v^{(c)}$ is induced in the AFM state, which reflects the breaking of the fourfold rotational symmetry. In other words, $T_y^{(c)}$ and $Q_v^{(c)}$ belong to the same irreducible representation in the AFM state.

Next we discuss the effect of the magnetic field, whose magnitude is set to be $|\mathbf{H}^{(el)}| = 0.01$. The results are shown in Figs. 2(g)–2(i) in the case of the [001] field and in Figs. 2(j)–2(l) in the case of the [100] field. There are two important observations in the magnetic field. The first one is that additional multipole moments other than the magnetic dipole moments $\mathbf{M}^{(c)}$ are induced according to the lowering of the crystal symmetry by the magnetic field. For example, in the Q_v -type AFQ state, the magnetic quadrupole moment $M_v^{(c)}$ becomes nonzero for the field along the [001] direction in Fig. 2(g), while nonzero $Q_v^{(c)}$, $Q_z^{(c)}$, and $T_y^{(c)}$ are induced for that along the [100] direction in Fig. 2(j). The second one is that the additional multipole moments induced by the magnetic field are much smaller than primary odd-parity multipole moments, which indicates that the additional multipoles lead to the small quantitative change in the NQR and NMR spectra. We summarize the active multipole moments induced by the AFQ and AFM orderings at zero and nonzero fields in Table II. The obtained results are consistent with those attained by the symmetry analysis.

III. HYPERFINE FIELD OF THE ^{59}Co NUCLEUS

We discuss the hyperfine field acting on the nuclear spins of ^{59}Co ions through effective multipole fields generated in Eq. (1). In general, the hyperfine field up to the second order of the nuclear spin with $I \geq 1$ is given by [72]

$$\mathcal{H} = -\gamma \hbar \mathbf{H} \cdot \hat{\mathbf{I}} + \frac{e^2 q Q}{4I(2I-1)} [3\hat{I}_z^2 - \hat{I}^2 + \eta(\hat{I}_x^2 - \hat{I}_y^2)], \quad (2)$$

where $\hat{\mathbf{I}} = (\hat{I}_X, \hat{I}_Y, \hat{I}_Z)$ is the nuclear spin operator with the principal axes of the local electric-field gradient at the Co nuclear site, (X, Y, Z) . The magnitude of $\hat{\mathbf{I}}$ is given by $I = 7/2$ for the ^{59}Co nucleus. The first term represents the Zeeman coupling term; γ and \hbar represent the gyromagnetic ratio and Dirac's constant, respectively. The second term describes the nuclear quadrupole interaction; e is the electric charge, q is the electric-field gradient parameter, Q is the nuclear electric quadrupole moment, and η is the anisotropic parameter. The amplitudes of \mathbf{H} , q , and η depend on electronic multipole moments at four neighboring Ce sites [Fig. 1(c)] as well as the external magnetic field and crystal-field potential. When we define $\mathbf{H}^{(n)} \equiv \gamma \hbar \mathbf{H}$, the energy scale of the nuclear system is compared with that of the electronic system as $\mathbf{H}^{(n)}/\mathbf{H}^{(el)} \sim 10^{-4}$. We rewrite the Hamiltonian in Eq. (2) in terms of the crystal axis coordinates (x, y, z) [see also Fig. 1(a)] as

$$\mathcal{H} = \mathbf{C} \cdot \hat{\mathbf{I}} + C_u \hat{I}_u + C_v \hat{I}_v + C_{yz} \hat{I}_{yz} + C_{zx} \hat{I}_{zx} + C_{xy} \hat{I}_{xy}, \quad (3)$$

where

$$\hat{I}_u = \frac{1}{2}(3\hat{I}_z^2 - \hat{I}^2), \quad (4)$$

$$\hat{I}_v = \frac{\sqrt{3}}{2}(\hat{I}_x^2 - \hat{I}_y^2), \quad (5)$$

$$\hat{I}_{yz} = \frac{\sqrt{3}}{2}(\hat{I}_y \hat{I}_z + \hat{I}_z \hat{I}_y), \quad (6)$$

$$\hat{I}_{zx} = \frac{\sqrt{3}}{2}(\hat{I}_z \hat{I}_x + \hat{I}_x \hat{I}_z), \quad (7)$$

$$\hat{I}_{xy} = \frac{\sqrt{3}}{2}(\hat{I}_x \hat{I}_y + \hat{I}_y \hat{I}_x). \quad (8)$$

The coupling constants for the effective magnetic field and electric-field gradient are parametrized as $\mathbf{C} = (C_x, C_y, C_z)$ and $(C_u, C_v, C_{yz}, C_{zx}, C_{xy})$, respectively. Among them, C_μ ($\mu = x, y, z$) includes two contributions from the external field $H_\mu^{(n)}$ and the internal dipole field C_μ^{el} from the electronic multipoles as

$$C_\mu = -\mathbf{H}^{(n)} + C_\mu^{el}, \quad (9)$$

whereas C_ν ($\nu = u, v, yz, zx, xy$) consists of two contributions from the crystal-field potential C_ν^{CF} and the internal quadrupole field C_ν^{el} from the electronic multipoles as

$$C_\nu = C_\nu^{CF} + C_\nu^{el}. \quad (10)$$

In Eqs. (9) and (10), C_μ^{el} and C_ν^{el} depend on the types of multipole orderings, which become nonzero through the effective hyperfine coupling between the electronic multipoles and nuclear spins or quadrupoles.

In the following sections, we focus on the multipole contributions to the effective hyperfine field by setting $C_\nu^{CF} = 0$ for

TABLE III. Irreducible representations of nuclear multipoles (NMP) and electronic cluster multipoles (CMP) in the local symmetry of the Co site in zero and nonzero magnetic fields \mathbf{H} . Here $X_{\pm} \equiv X_x \pm nX_y$ and $X_{2\pm} \equiv X_{yz} \pm nX_{zx}$ for $X = I, Q^{(c)}, M^{(c)}, T^{(c)}$ and $n = i(1)$ for $\bar{4}m'2'$ ($2'2'2', 2'$). For $\mathbf{H}_{\parallel[001]}$, the multipoles in the square brackets are also activated. The irreducible representations of a magnetic point group are represented by using the irreducible representations of its unitary subgroup, which is shown below the respective magnetic point groups [74]. The superscript \pm of the irreducible representation is the parity with respect to the antilinear-unitary operation (even + and odd -). The axes of the twofold rotation C_2 of $2'2'2'$ and $\mathcal{T}C_2$ of $2'$ in $\mathbf{H}_{\perp[001]}$ ($\mathbf{H}_{\perp[\bar{1}10]}$) are along $[110]$ and $[001]$ ($[\bar{1}10]$), respectively. The mirror plane in m' is normal to the $[010]$ direction.

NMP	CMP	$\bar{4}m'2'$	$\mathbf{H}_{\parallel[001]}$	$\mathbf{H}_{\parallel[100]}$	$\mathbf{H}_{\parallel[110]}$	$\mathbf{H}_{\perp[001]}$	$\mathbf{H}_{\perp[010]}$	$\mathbf{H}_{\perp[\bar{1}10]}$
		($\bar{4}m2$)	($\bar{4}$)	(m)	(2)	(1)	(1)	(1)
I_u	$Q_u^{(c)}, G_{xy}^{(c)}$	A_1^+	A^+	A'^+	A^+	A^+	A^+	A^+
	$G_v^{(c)}$	A_2^+	A^-	A''^+	B^-	A^+	A^-	A^-
I_{xy}	$Q_{xy}^{(c)}$	B_1^+	B^+	A''^+	A^+	A^+	A^-	A^+
I_v	$Q_v^{(c)}, Q_z^{(c)}$	B_2^+	B^-	A'^+	B^-	A^+	A^+	A^-
I_{yz}	$Q_{yz}^{(c)}$	E^+		A'^-		A^-	A^-	
I_{zx}	$Q_{zx}^{(c)}$			A''^-		A^-	A^+	
	$Q_x^{(c)}$	E^+		A''^-		A^-	A^+	
	$Q_y^{(c)}$			A'^-		A^-	A^-	
I_{2+}	$Q_{2+}^{(c)} [iQ_+^{(c)}]$		$E^{(2)+}$		B^+	A^-		A^+
I_{2-}	$Q_{2-}^{(c)} [iQ_-^{(c)}]$		$E^{(1)+}$		A^-	A^-		A^-
$[iI_{2+}]$	$Q_+^{(c)} [iQ_{2+}^{(c)}]$		$E^{(2)-}$		A^-	A^-		A^-
$[iI_{2-}]$	$Q_-^{(c)} [iQ_{2-}^{(c)}]$		$E^{(1)-}$		B^+	A^-		A^+
	$M_{xy}^{(c)}$	A_1^-	A^-	A'^-	A^-	A^-	A^-	A^-
I_z	$M_z^{(c)}, M_v^{(c)}$	A_2^-	A^+	A''^-	B^+	A^-	A^+	A^+
	$M_z^{\beta(c)}, M_u^{(c)}$	B_1^-	B^-	A''^-	A^-	A^-	A^+	A^-
	$M_{xyz}^{(c)}$	B_2^-	B^+	A'^-	B^+	A^-	A^-	A^+
I_x	$M_x^{(c)}$	E^-		A'^+		A^+	A^+	
I_y	$M_y^{(c)}$			A''^+		A^+	A^-	
	$T_x^{(c)}$	E^-		A''^+		A^+	A^-	
	$T_y^{(c)}$			A'^+		A^+	A^+	
I_+	$M_+^{(c)} [iT_-^{(c)}]$		$E^{(1)-}$		A^+	A^+		A^+
I_-	$M_-^{(c)} [iT_+^{(c)}]$		$E^{(2)-}$		B^-	A^+		A^-
$[iI_-]$	$T_+^{(c)} [iM_-^{(c)}]$		$E^{(2)+}$		A^+	A^+		A^+
$[iI_+]$	$T_-^{(c)} [iM_+^{(c)}]$		$E^{(1)+}$		B^-	A^+		A^-

simplicity [73]. We show an effective Hamiltonian for the Co nucleus in multipole fields from Ce sites in the zero magnetic field in Sec. III A and in finite magnetic fields in Sec. III B.

A. Zero magnetic field

Before discussing the effect of odd-parity multipoles, we start from the hyperfine field in the paramagnetic state. In the paramagnetic state in the zero magnetic field, only the electric quadrupole $Q_u^{(c)}$ becomes finite among the electronic multipoles, which corresponds to the second term in Eq. (3), as shown in Table II. The nuclear Hamiltonian at the single Co site is given by

$$\mathcal{H}_{\text{para}} = C_u^{\text{el}} \hat{I}_u \equiv c_u^e Q_u^{(c)} \hat{I}_u, \quad (11)$$

where the coupling constant C_u^{el} is represented by the product of the hyperfine coupling constant c_u^e and the thermal average of the cluster electronic multipole $Q_u^{(c)}$, $C_u^{\text{el}} = c_u^e Q_u^{(c)}$. Here and hereafter, the superscript and subscript in c_μ^p represent the even- or odd-parity ($p = e$ or o) multipoles and the type

of coupled nuclear multipoles ($\mu = x, y, z, u, v, yz, zx, xy$), respectively.

The other terms in Eq. (3) become nonzero once the electronic multipole orderings occur, i.e., for nonzero h_X^s in Eq. (1). One can derive the effective hyperfine field in the multipole orderings on the basis of magnetic point group symmetry, as it consists of the coupling terms belonging to the totally symmetric representation of $\bar{4}m'2'$. We display the irreducible representations of the cluster multipoles and nuclear multipoles in Table III.

The general form of the effective hyperfine field in the odd-parity multipole orders is given by

$$\begin{aligned} \mathcal{H}_{\text{order}}^o = & c_z^o M_v^{(c)} \hat{I}_z + c_{x,y}^o (T_y^{(c)} \hat{I}_x + T_x^{(c)} \hat{I}_y) + c_u^o G_{xy}^{(c)} \hat{I}_u \\ & + c_v^o Q_z^{(c)} \hat{I}_v + c_{yz,zx}^o (Q_y^{(c)} \hat{I}_{yz} - Q_x^{(c)} \hat{I}_{zx}), \end{aligned} \quad (12)$$

$$\begin{aligned} \mathcal{H}_{\text{order}}^e = & c_z^e M_z^{(c)} \hat{I}_z + c_{x,y}^e (M_x^{(c)} \hat{I}_x + M_y^{(c)} \hat{I}_y) + c_{xy}^e Q_{xy}^{(c)} \hat{I}_{xy} \\ & + c_v^e Q_v^{(c)} \hat{I}_v + c_{yz,zx}^e (Q_{yz}^{(c)} \hat{I}_{yz} + Q_{zx}^{(c)} \hat{I}_{zx}), \end{aligned} \quad (13)$$

where $\mathcal{H}_{\text{order}}^{\text{o}}$ ($\mathcal{H}_{\text{order}}^{\text{e}}$) stands for the hyperfine field in the presence of odd-parity (even-parity) multipoles. Interestingly, the effective hyperfine field includes the coupling between electronic odd-parity multipoles and nuclear even-parity multipoles owing to the lack of the local inversion symmetry at the Co site. The hyperfine fields in Eqs. (11)–(13) are summarized in Table IV(a).

In CeCoSi, there are two Co ions in the unit cell, which are connected by the fourfold rotation. As the signs of the odd-parity crystal field of two Co ions are opposite while those of the even-parity one are the same, the total nuclear Hamiltonian in a unit cell is given by

$$\mathcal{H}_{\text{Co}} = \mathcal{H}_{\text{CoA}} + \mathcal{H}_{\text{CoB}}, \quad (14)$$

$$\mathcal{H}_{\text{CoA}} = \mathcal{H}_{\text{para}} + \mathcal{H}_{\text{order}}^{\text{o}} + \mathcal{H}_{\text{order}}^{\text{e}}, \quad (15)$$

$$\mathcal{H}_{\text{CoB}} = \mathcal{H}_{\text{para}} - \mathcal{H}_{\text{order}}^{\text{o}} + \mathcal{H}_{\text{order}}^{\text{e}}. \quad (16)$$

The different sign of $\mathcal{H}_{\text{order}}^{\text{o}}$ for the different sublattices is an important outcome of odd-parity multipoles. In other words, the presence of the sublattice-dependent splitting of the resonant spectrum corresponds to the emergent odd-parity multipoles within the $\mathbf{q} = \mathbf{0}$ orders, as shown in Secs. IV and V. The obtained hyperfine field including the odd-parity multipole moments in Eq. (12) is one of the main results in this paper.

B. Magnetic field

At an external magnetic field, a Zeeman term is taken into account, which is given by

$$\mathcal{H}_{\text{Zeeman}} = -\mathbf{H}^{(n)} \cdot \hat{\mathbf{I}}. \quad (17)$$

Although the Zeeman term induces the magnetic dipole contribution, it also induces additional electronic multipole contributions according to the lowering of the symmetry.

By considering the magnetic field along the [001] direction, additional hyperfine field terms appear as

$$\tilde{\mathcal{H}}_{\text{para}}^{[001]} = \tilde{c}_z^{\text{e}} Q_u^{(c)} \hat{I}_z + \tilde{c}_u^{\text{e}} M_z^{(c)} \hat{I}_u, \quad (18)$$

$$\begin{aligned} \tilde{\mathcal{H}}_{\text{order}}^{\text{o}[001]} &= \tilde{c}_z^{\text{o}} G_{xy}^{(c)} \hat{I}_z + \tilde{c}_{x,y}^{\text{o}} (Q_x^{(c)} \hat{I}_x - Q_y^{(c)} \hat{I}_y) + \tilde{c}_u^{\text{o}} M_v^{(c)} \hat{I}_u \\ &+ \tilde{c}_v^{\text{o}} M_u^{(c)} \hat{I}_v + \tilde{c}_{yz,zx}^{\text{o}} (T_x^{(c)} \hat{I}_{yz} + T_y^{(c)} \hat{I}_{zx}), \end{aligned} \quad (19)$$

$$\begin{aligned} \tilde{\mathcal{H}}_{\text{order}}^{\text{e}[001]} &= \tilde{c}_{x,y}^{\text{e}} (Q_{zx}^{(c)} \hat{I}_x + Q_{yz}^{(c)} \hat{I}_y) + \tilde{c}_{xy}^{\text{e}} M_{xyz}^{(c)} \hat{I}_{xy} \\ &+ \tilde{c}_v^{\text{e}} M_z^{\beta(c)} \hat{I}_v + \tilde{c}_{yz,zx}^{\text{e}} (M_y^{(c)} \hat{I}_{yz} + M_x^{(c)} \hat{I}_{zx}), \end{aligned} \quad (20)$$

where $\tilde{\mathcal{H}}_{\text{para}}^{[001]}$ is the additional hyperfine field induced by the magnetic field in the paramagnetic state, while $\tilde{\mathcal{H}}_{\text{order}}^{\text{o}[001]}$ ($\tilde{\mathcal{H}}_{\text{order}}^{\text{e}[001]}$) is the additional hyperfine field in the presence of the odd-parity (even-parity) multipole orderings. In addition, \tilde{c}_μ^p ($p = \text{e or o}$ and $\mu = u, v, yz, zx, xy$) is a magnetic-field-dependent coupling constant, which vanishes without the magnetic field.

The appearance of various multipole contributions in Eqs. (18)–(20) is due to the reduction of the local symmetry at the Co site $4m21' \rightarrow 4m'2'$. Reflecting the breaking of the time-reversal symmetry, the effective couplings between

TABLE IV. (a) Hyperfine field at zero magnetic field. (b) and (c) Additional hyperfine field terms in the magnetic field along the (b) [001] and (c) [100] directions. The coupling constants are real.

	C_x^{el}	C_y^{el}	C_z^{el}	C_u^{el}	C_v^{el}	C_{yz}^{el}	C_{zx}^{el}	C_{xy}^{el}
(a) Zero magnetic field								
$\mathcal{H}_{\text{para}}^{\text{o}}$								
$\mathcal{H}_{\text{order}}^{\text{o}}$	$c_{x,y}^{\text{o}} T_x^{(c)}$			$c_u^{\text{o}} Q_z^{(c)}$	$c_v^{\text{o}} Q_z^{(c)}$	$c_{yz,zx}^{\text{o}} Q_y^{(c)}$	$-c_{yz,zx}^{\text{o}} Q_x^{(c)}$	
$\mathcal{H}_{\text{order}}^{\text{e}}$	$c_{x,y}^{\text{e}} M_x^{(c)}$		$c_z^{\text{e}} M_z^{(c)}$	$c_u^{\text{e}} Q_u^{(c)}$	$c_v^{\text{e}} Q_u^{(c)}$	$c_{yz,zx}^{\text{e}} Q_{yz}^{(c)}$	$c_{yz,zx}^{\text{e}} Q_{zx}^{(c)}$	$c_{xy}^{\text{e}} Q_{xy}^{(c)}$
(b) [001] magnetic field								
$\mathcal{H}_{\text{para}}^{[001]}$				$\tilde{c}_z^{\text{e}} M_z^{(c)}$	$\tilde{c}_u^{\text{e}} M_u^{(c)}$			
$\mathcal{H}_{\text{order}}^{\text{o}[001]}$				$\tilde{c}_u^{\text{o}} M_u^{(c)}$	$\tilde{c}_v^{\text{o}} M_u^{(c)}$			
$\mathcal{H}_{\text{order}}^{\text{e}[001]}$			$-\tilde{c}_{x,y}^{\text{e}} Q_{xy}^{(c)}$			$\tilde{c}_{yz,zx}^{\text{e}} T_x^{(c)}$	$\tilde{c}_{yz,zx}^{\text{e}} T_y^{(c)}$	
(c) [100] magnetic field								
$\mathcal{H}_{\text{para}}^{[100]}$	$\tilde{c}_x^{\text{e-1}} Q_u^{(c)} + \tilde{c}_x^{\text{e-2}} Q_v^{(c)}$			$\tilde{c}_u^{\text{e-1}} Q_u^{(c)} + \tilde{c}_u^{\text{e-2}} M_x^{(c)}$	$\tilde{c}_v^{\text{e-1}} Q_u^{(c)} + \tilde{c}_v^{\text{e-2}} M_x^{(c)}$			
$\mathcal{H}_{\text{order}}^{\text{o}[100]}$	$\tilde{c}_x^{\text{o-1}} Q_z^{(c)} + \tilde{c}_x^{\text{o-2}} G_{xy}^{(c)}$		$\tilde{c}_z^{\text{o-1}} Q_x^{(c)} + \tilde{c}_z^{\text{o-2}} M_u^{(c)}$	$\tilde{c}_u^{\text{o-1}} Q_z^{(c)} + \tilde{c}_u^{\text{o-2}} T_y^{(c)}$	$\tilde{c}_v^{\text{o-1}} G_{xy}^{(c)} + \tilde{c}_v^{\text{o-2}} T_y^{(c)}$	$\tilde{c}_{yz}^{\text{o-1}} Q_y^{(c)} + \tilde{c}_{yz}^{\text{o-2}} M_{xy}^{(c)}$	$\tilde{c}_{zx}^{\text{o-1}} M_u^{(c)} + \tilde{c}_{zx}^{\text{o-2}} M_u^{(c)}$	$\tilde{c}_{xy}^{\text{o-1}} G_u^{(c)} + \tilde{c}_{xy}^{\text{o-2}} T_x^{(c)}$
$\mathcal{H}_{\text{order}}^{\text{e}[100]}$	$\tilde{c}_x^{\text{e-1}} Q_{xy}^{(c)} + \tilde{c}_x^{\text{e-2}} M_y^{(c)}$		$\tilde{c}_z^{\text{e-1}} Q_{zx}^{(c)} + \tilde{c}_z^{\text{e-2}} M_z^{\beta(c)}$	$\tilde{c}_u^{\text{e-1}} Q_{yz}^{(c)} + \tilde{c}_u^{\text{e-2}} M_{xy}^{(c)}$	$\tilde{c}_v^{\text{e-1}} Q_{yz}^{(c)} + \tilde{c}_v^{\text{e-2}} M_{xy}^{(c)}$	$\tilde{c}_{yz}^{\text{e-1}} Q_{yz}^{(c)} + \tilde{c}_{yz}^{\text{e-2}} M_z^{\beta(c)}$	$\tilde{c}_{zx}^{\text{e-1}} M_z^{(c)} + \tilde{c}_{zx}^{\text{e-2}} M_z^{\beta(c)}$	$\tilde{c}_{xy}^{\text{e-1}} M^{(c)} + \tilde{c}_{xy}^{\text{e-2}} M^{(c)}$

electronic and nuclear multipoles with opposite time-reversal parity appear. In other words, the electric (magnetic) multipole at the Ce site is coupled with the nuclear dipole (quadrupole) at the Co site. From a microscopic viewpoint, such a coupling originates from the magnetic multipoles with spatially anisotropic distributions, such as magnetic octupoles, which are described by the coupling between the anisotropic charge distribution and the magnetic moment

[36,38]. For instance, in the case of the Q_v -type ordering in the magnetic field along the [001] direction, the magnetic quadrupole $M_v^{(c)}$ with odd time reversal is induced as shown in Fig. 2(g). Since $M_v^{(c)}$ belongs to the same irreducible representation A^+ as I_u with even time reversal in the magnetic point group $\bar{4}m'2'$ from Table III, the field-induced $M_v^{(c)}$ affects the $(3z^2 - r^2)$ -type charge distribution and results in the effective coupling between $M_v^{(c)}$ and I_u .

Similarly, the additional hyperfine fields in the [100] magnetic field are given by

$$\tilde{\mathcal{H}}_{\text{para}}^{[100]} = (\tilde{c}_x^{e,1} Q_u^{(c)} + \tilde{c}_x^{e,2} Q_v^{(c)}) \hat{I}_x + (\tilde{c}_u^{e,1} Q_v^{(c)} + \tilde{c}_u^{e,2} M_x^{(c)}) \hat{I}_u + (\tilde{c}_v^{e,1} Q_u^{(c)} + \tilde{c}_v^{e,2} M_x^{(c)}) \hat{I}_v, \quad (21)$$

$$\begin{aligned} \tilde{\mathcal{H}}_{\text{order}}^{[100]} = & (\tilde{c}_x^{o,1} Q_z^{(c)} + \tilde{c}_x^{o,2} G_{xy}^{(c)}) \hat{I}_x + (\tilde{c}_y^{o,1} G_v^{(c)} + \tilde{c}_y^{o,2} T_x^{(c)}) \hat{I}_y + (\tilde{c}_z^{o,1} Q_x^{(c)} + \tilde{c}_z^{o,2} M_u^{(c)}) \hat{I}_z + (\tilde{c}_u^{o,1} Q_z^{(c)} + \tilde{c}_u^{o,2} T_y^{(c)}) \hat{I}_u \\ & + (\tilde{c}_v^{o,1} G_{xy}^{(c)} + \tilde{c}_v^{o,2} T_y^{(c)}) \hat{I}_v + (\tilde{c}_{yz}^{o,1} Q_y^{(c)} + \tilde{c}_{yz}^{o,2} M_{xy}^{(c)}) \hat{I}_{yz} + (\tilde{c}_{zx}^{o,1} M_u^{(c)} + \tilde{c}_{zx}^{o,2} M_v^{(c)}) \hat{I}_{zx} + (\tilde{c}_{xy}^{o,1} G_v^{(c)} + \tilde{c}_{xy}^{o,2} T_x^{(c)}) \hat{I}_{xy}, \end{aligned} \quad (22)$$

$$\tilde{\mathcal{H}}_{\text{order}}^{e[100]} = (\tilde{c}_y^{e,1} Q_{xy}^{(c)} + \tilde{c}_y^{e,2} M_y^{(c)}) \hat{I}_y + (\tilde{c}_z^{e,1} Q_{zx}^{(c)} + \tilde{c}_z^{e,2} M_z^{\beta(c)}) \hat{I}_z + (\tilde{c}_{yz}^{e,1} Q_{yz}^{(c)} + \tilde{c}_{yz}^{e,2} M_{xyz}^{(c)}) \hat{I}_{yz} + (\tilde{c}_{zx}^{e,1} M_z^{(c)} + \tilde{c}_{zx}^{e,2} M_z^{\beta(c)}) \hat{I}_{zx} + \tilde{c}_{xy}^e M_y^{(c)} \hat{I}_{xy}, \quad (23)$$

where the local symmetry at the Co site reduces as $\bar{4}m21' \rightarrow 2'mm'$. For in-plane fields, the \hat{I}_v term additionally contributes to $\tilde{\mathcal{H}}_{\text{para}}^{[100]}$ due to the breaking of the fourfold improper rotational symmetry.

The additional hyperfine field Hamiltonian in the external magnetic field is summarized in Tables IV(b) and IV(c). One can obtain the hyperfine field Hamiltonian for other field directions by using the irreducible representation in Table III.

In the end, the total Hamiltonian in a unit cell in the magnetic field is given by

$$\mathcal{H}_{\text{Co}} = \mathcal{H}_{\text{CoA}} + \mathcal{H}_{\text{CoB}} + \tilde{\mathcal{H}}_{\text{CoA}} + \tilde{\mathcal{H}}_{\text{CoB}}, \quad (24)$$

$$\mathcal{H}_{\text{CoA}} = \mathcal{H}_{\text{Zeeman}} + \mathcal{H}_{\text{para}} + \mathcal{H}_{\text{order}}^o + \mathcal{H}_{\text{order}}^e, \quad (25)$$

$$\mathcal{H}_{\text{CoB}} = \mathcal{H}_{\text{Zeeman}} + \mathcal{H}_{\text{para}} - \mathcal{H}_{\text{order}}^o + \mathcal{H}_{\text{order}}^e, \quad (26)$$

$$\tilde{\mathcal{H}}_{\text{CoA}} = \tilde{\mathcal{H}}_{\text{para}} + \tilde{\mathcal{H}}_{\text{order}}^o + \tilde{\mathcal{H}}_{\text{order}}^e, \quad (27)$$

$$\tilde{\mathcal{H}}_{\text{CoB}} = \tilde{\mathcal{H}}_{\text{para}} - \tilde{\mathcal{H}}_{\text{order}}^o + \tilde{\mathcal{H}}_{\text{order}}^e. \quad (28)$$

We use the above nuclear Hamiltonian \mathcal{H}_{Co} to examine the NMR spectra in the odd-parity multipole orderings in the following sections.

IV. NQR SPECTRA AT ZERO FIELD

We examine how odd-parity multipole moments affect an NQR spectrum. In the paramagnetic state, the nuclear Hamiltonian given by Eq. (14) leads to three NQR frequencies $f = \nu_Q, 2\nu_Q,$ and $3\nu_Q$, where $\hbar\nu_Q = 3c_u^e Q_u^{(c)}$. We take $\nu_Q = 1$ as the frequency unit.

In the following, we show the resonance frequencies in odd-parity multipole orderings in Secs. IV A–IV C: the Q_v -type AFQ state with $G_{xy}^{(c)}$ in Sec. IV A, the Q_u -type AFQ state with $Q_z^{(c)}$ in Sec. IV B, and the M_x -type AFM state with $T_y^{(c)}$ in Sec. IV C. In the calculations, we set the coupling constant in Eqs. (11) and (12) as $c_u^e = c_Q$, which is estimated from the NQR frequency in Ref. [75] as $c_Q = 0.13$ when setting $\gamma\hbar = 1$, while the coupling constants are set to be c for the pri-

marily induced multipoles and c' for the secondarily induced multipoles as the unknown model parameters for simplicity.

A. Staggered Q_v -type AFQ

We discuss the NQR spectrum in the staggered Q_v -type AFQ state, where the effective nuclear Hamiltonian is represented by considering the finite electronic multipoles in Eqs. (11)–(13) as

$$\mathcal{H}_{\text{CoA(B)}} = (c_Q Q_u^{(c)} \pm c G_{xy}^{(c)}) \hat{I}_u. \quad (29)$$

The positive (negative) sign in the second term corresponds to $\mathcal{H}_{\text{CoA}} (\mathcal{H}_{\text{CoB}})$.

The NQR frequencies of Co_A and Co_B sites as a function of $G_{xy}^{(c)}$ with fixed $c = 0.02$ are shown in Fig. 3(a). The color scale in Fig. 3 shows the intensity of the NQR spectrum, which is calculated by the magnitude of the matrix element of I_x between different nuclear states i and j at the Co_{A(B)} site, $|\tilde{I}_{x,A(B)}^{ij}|^2 \equiv |\langle i | \tilde{I}_{x,A(B)} | j \rangle|^2$, where \tilde{I}_μ ($\mu = x, y, z$) represents the normalized I_μ satisfying $\text{Tr}[\tilde{I}_\mu \tilde{I}_\mu^\dagger] = 1$.

The result shows that the NQR frequencies for Co_A and Co_B have different values and show the spectral splittings and shift in the Q_v -type AFQ state. The sublattice-dependent splitting is due to the effective coupling between $G_{xy}^{(c)}$ and I_u with different signs for different sublattices. In other words, the odd-parity multipole moment $G_{xy}^{(c)}$ in Eq. (29) plays a significant role in the splitting of the NQR frequencies. In fact, the splittings of the NQR frequencies are proportional to $G_{xy}^{(c)}$. On the other hand, the shift of the frequency to smaller f is due to the decrease of the dominant $c_Q Q_u^{(c)}$ ($c_Q \gg c$) term in Eq. (29) by the suppression of $Q_u^{(c)}$ while increasing $G_{xy}^{(c)}$ as shown in Fig. 2(d). Note that it might be difficult to detect the splitting due to the odd-parity multipoles even for a saturated multipole moment $G_{xy}^{(c)} \sim 0.5$ when the coupling constant c is small, since the splittings are proportional to $c G_{xy}^{(c)}$.

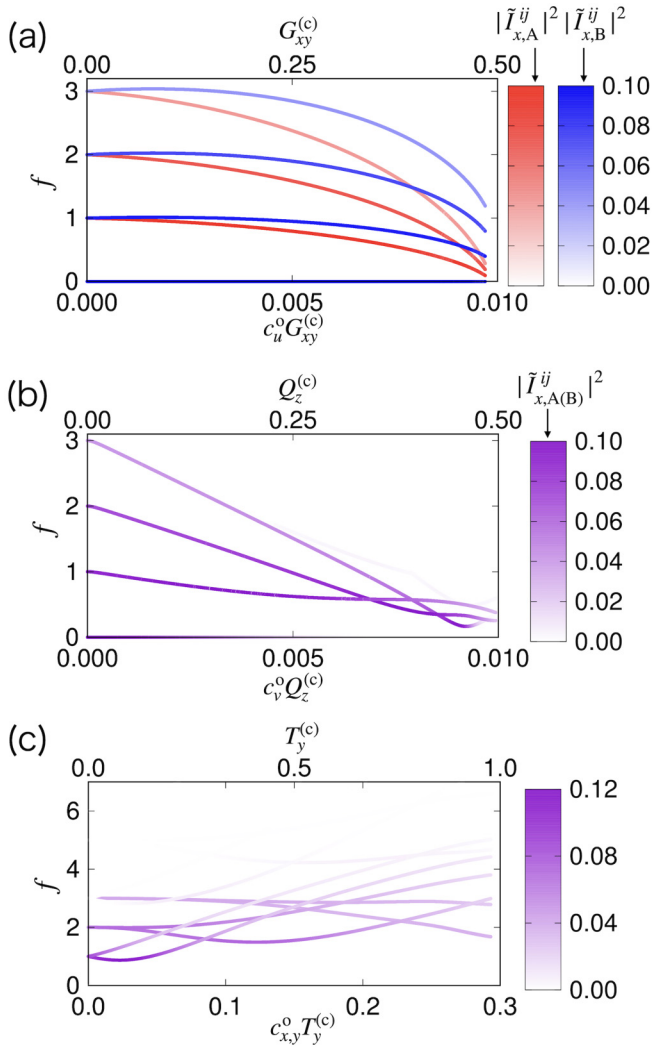


FIG. 3. Odd-parity multipole (upper scale) and its hyperfine field (lower scale) dependences of the NQR frequency f in the staggered (a) Q_v -type AFQ, (b) Q_u -type AFQ, and (c) M_x -type AFM states. The coupling constants c_u^o , c_v^o , and $c_{x,y}^o$ are set as $c_u^o = c_v^o = c = 0.02$ in the AFQ states and $c_{x,y}^o = c = 0.3$ in the AFM state. Other coupling constants are set to be $c' = 0.02$. As an intensity of the spectrum, $|\tilde{I}_{x,A(B)}^{ij}|^2$ is shown by the colorplot in red (blue) for the Co_A (Co_B) site. When the spectra from Co_A and Co_B are equivalent, their intensities are shown by violet.

B. Staggered Q_u -type AFQ

In the staggered Q_u -type AFQ state with $Q_z^{(c)}$, the effective nuclear Hamiltonians of Co_A and Co_B are represented by

$$\mathcal{H}_{\text{Co}_{A(B)}} = c_Q Q_u^{(c)} \hat{I}_u \pm c Q_z^{(c)} \hat{I}_v. \quad (30)$$

The NQR spectrum for the coupling constant $c = 0.02$ is shown in Fig. 3(b). In contrast to the result in the Q_v -type AFQ state, there is no splitting in the NQR spectrum. This is because the different sign of $Q_z^{(c)}$ in Eq. (30) is not relevant to the splitting, which is consistent with the symmetry argument that there is no linear coupling between $Q_z^{(c)}$ and $Q_u^{(c)}$ in the free-energy expansion at the Co site. In the end, nonzero $Q_z^{(c)}$ just affects the spectral shift.

In addition to the splitting, the difference is found in the odd-parity multipole dependence of the frequency shift. The frequencies in the Q_u -type AFQ state in Fig. 3(b) decrease with increasing $Q_z^{(c)}$ faster than those in the Q_v -type AFQ state in Fig. 3(a). This is understood from the different dependences on the multipole moments as discussed in Sec. II C; $Q_u^{(c)}$ in the Q_u -type AFQ state decreases by $\sim [Q_z^{(c)}]^{4/3}$, while that in the Q_v -type AFQ state decreases by $\sim [G_{xy}^{(c)}]^2$.

C. Staggered M_x -type AFM

In the staggered M_x -type AFM state, the nuclear Hamiltonian is represented by

$$\mathcal{H}_{\text{Co}_{A(B)}} = \pm c T_y^{(c)} \hat{I}_x + c_Q Q_u^{(c)} \hat{I}_u + c' Q_v^{(c)} \hat{I}_v. \quad (31)$$

It should be noted that nuclear dipole contribution in the M_x -type AFM appears even without the net magnetization or the magnetic field. Figure 3(c) shows the NQR spectrum for the coupling constants $c = 0.3$ and $c' = 0.02$ in the M_x -type AFM state, where c is estimated from the magnitude of the internal magnetic field in Ref. [75]. The NQR frequencies split into seven due to the contribution from the internal magnetic field arising from the first term in Eq. (31). Meanwhile, the NQR frequencies for Co_A and Co_B sites are the same, which indicates that there is no sublattice-dependent splitting in the presence of the odd-parity $T_y^{(c)}$. This means that $T_y^{(c)}$ does not linearly couple with $Q_u^{(c)}$ in the free-energy expansion, which is consistent with the symmetry argument. Thus, it is difficult to conclude the presence of $T_y^{(c)}$ only from the seven splittings in Fig. 3(c). In fact, the NQR spectra split into seven can be obtained in the even-parity magnetic dipole order, such as $M_x^{(c)}$, in Table I.

V. NMR SPECTRA

In this section we discuss the NMR spectra in the odd-parity multipole orderings. The applied resonance fields are along the [001] and [100] directions in Secs. V A and V B, respectively. We set $\gamma \hbar = 1$ and $|\mathbf{H}^{(n)}| = 1$. The coupling constants are set as $c_u^e = c_Q = 0.13$ as well as that in NQR in Sec. IV. The other coupling constants are set to be c for the primarily induced multipoles and c' for the secondarily induced multipoles for simplicity. The field-swept spectra are shown in Appendix B.

A. The [001]-field spectrum

We discuss the NMR spectra in the paramagnetic state, Q_v -type AFQ state, Q_u -type AFQ state, and M_x -type AFM state in Secs. V A 1–V A 4, respectively.

1. Paramagnetic state

In the paramagnetic state in the [001] magnetic field $\mathbf{H}^{(n)} = (0, 0, H_z^{(n)})$, the effective nuclear Hamiltonian is represented by

$$\mathcal{H}_{\text{Co}_{A(B)}} = (-H_z^{(n)} + c' M_z^{(c)}) \hat{I}_z + c_Q Q_u^{(c)} \hat{I}_u, \quad (32)$$

$$\tilde{\mathcal{H}}_{\text{Co}_{A(B)}} = c' Q_u^{(c)} \hat{I}_z + c' M_z^{(c)} \hat{I}_u. \quad (33)$$

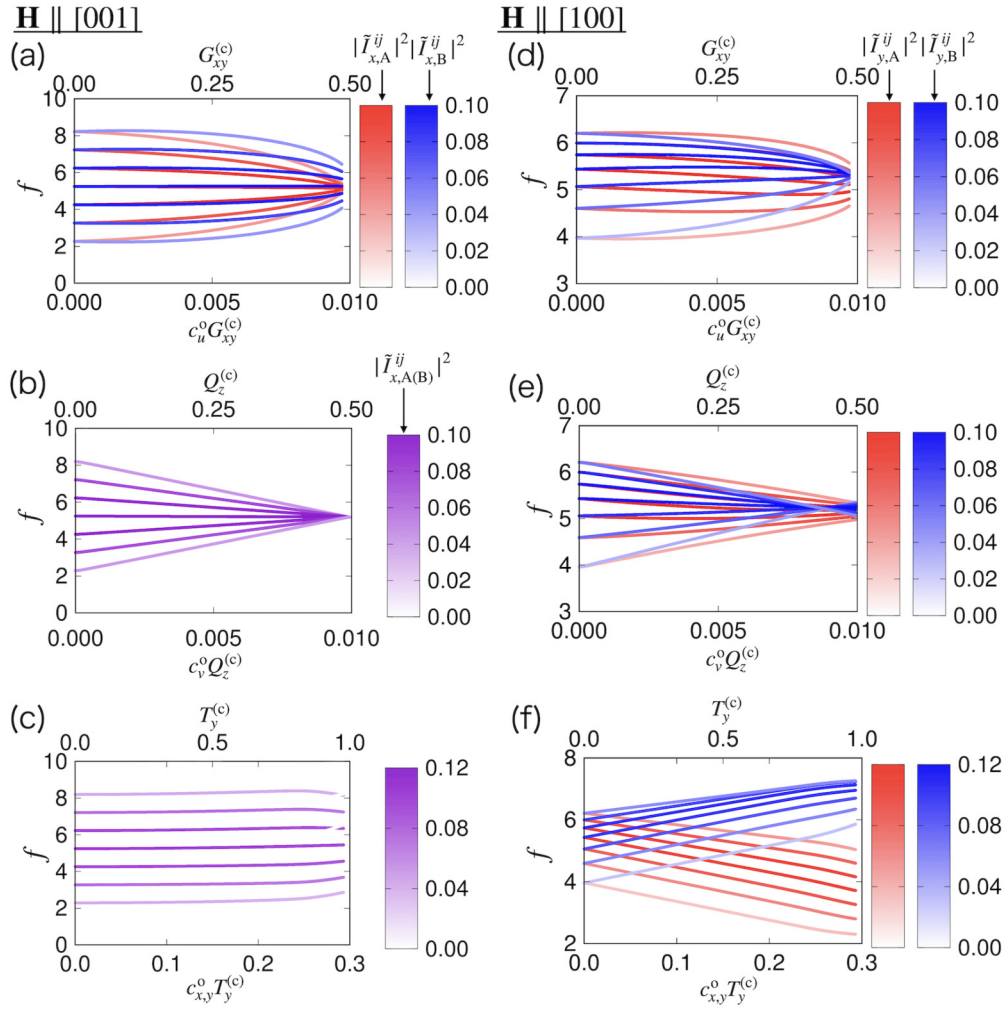


FIG. 4. Odd-parity multipole dependences of the NMR frequency f in (a)–(c) the [001] magnetic field and (d)–(f) the [100] magnetic field. The data are for the (a) and (d) Q_v -type AFQ, (b) and (e) Q_u -type AFQ, and (c) and (f) M_x -type AFM states. The color scales represent the intensities with (a)–(c) $|\tilde{I}_{x,A(B)}^{ij}|^2$ and (d)–(f) $|\tilde{I}_{y,A(B)}^{ij}|^2$. The coupling constants are set as $c_u^o = c_v^o = c = 0.02$ in the AFQ states and $c_{x,y}^o = c = 0.3$ in the AFM state. Other coupling constants are set to be $c' = 0.02$.

The first term in Eq. (32) includes the Zeeman term from the external magnetic field. The sum of the external magnetic field and the hyperfine field in Eqs. (32) and (33) results in the seven spectral peaks separated by the same interval in the NMR measurement.

2. Staggered Q_v -type AFQ

In the Q_v -type AFQ state, the effective nuclear Hamiltonian is obtained as

$$\mathcal{H}_{\text{CoA(B)}} = (-H_z^{(n)} + c'M_z^{(c)})\hat{I}_z + (c_Q Q_u^{(c)} \pm cG_{xy}^{(c)})\hat{I}_u, \quad (34)$$

$$\tilde{\mathcal{H}}_{\text{CoA(B)}} = c'(Q_u^{(c)} \pm G_{xy}^{(c)} \pm M_v^{(c)})\hat{I}_z + c'(M_z^{(c)} \pm M_v^{(c)})\hat{I}_u. \quad (35)$$

The frequency-swept NMR spectrum for $c = c' = 0.02$ is shown in Fig. 4(a), where the color scale represents the intensity of the [001]-field NMR spectrum. Figure 4(a) shows that $G_{xy}^{(c)}$ leads to sublattice-dependent spectral splittings due to the different frequencies of Co_A and Co_B as well as the

result in NQR. The NMR spectrum is mainly determined by the following dominant contributions: the Zeeman term, the $c_Q Q_u^{(c)}$ term, and primarily induced $G_{xy}^{(c)}$ terms. The spectral splittings originate from the odd-parity multipoles $G_{xy}^{(c)}$ and $M_v^{(c)}$, which are coupled with $Q_u^{(c)}$ and $M_z^{(c)}$, though the contribution from $M_v^{(c)}$ is much smaller than that of $G_{xy}^{(c)}$, as discussed in Sec. II C. Additionally, each spectrum is shifted by $[G_{xy}^{(c)}]^2$ as discussed in Sec. IV B.

3. Staggered Q_u -type AFQ

In the Q_u -type AFQ state, the effective nuclear Hamiltonian is described as

$$\mathcal{H}_{\text{CoA(B)}} = (-H_z^{(n)} + c'M_z^{(c)})\hat{I}_z + c_Q Q_u^{(c)}\hat{I}_u \pm cQ_z^{(c)}\hat{I}_v, \quad (36)$$

$$\tilde{\mathcal{H}}_{\text{CoA(B)}} = c'Q_u^{(c)}\hat{I}_z + c'M_z^{(c)}\hat{I}_u \pm c'M_u^{(c)}\hat{I}_v. \quad (37)$$

The NMR spectrum for $c = c' = 0.02$ is shown in Fig. 4(b). The seven frequencies have no additional splitting for both Co sites, since the induced odd-parity multipoles $Q_z^{(c)}$ and $M_u^{(c)}$ in

TABLE V. Sublattice-dependent NQR and NMR splittings in the AFM, AFQ, and AFO states in the six field directions [001], [100], [110], \perp [001], \perp [010], and \perp [110]. The local multipoles (LMP) at the Ce site and cluster odd-parity multipoles (OPMP) are shown in the second and third columns, respectively. The mark \checkmark represents the presence of the sublattice-dependent splittings.

State	LMP	OPMP	NQR	NMR					
				$H_{\parallel[001]}$	$H_{\parallel[100]}$	$H_{\parallel[110]}$	$H_{\perp[001]}$	$H_{\perp[010]}$	$H_{\perp[110]}$
AFM	M_x	T_y			\checkmark	\checkmark	\checkmark	\checkmark	\checkmark
AFM	M_y	T_x				\checkmark	\checkmark		\checkmark
AFM	M_z	M_u						\checkmark	
AFQ	Q_u	Q_z			\checkmark		\checkmark	\checkmark	
AFQ	Q_v	G_{xy}	\checkmark	\checkmark	\checkmark	\checkmark	\checkmark	\checkmark	\checkmark
AFQ	Q_{xy}	G_v					\checkmark		
AFQ	Q_{yz}	Q_y							\checkmark
AFQ	Q_{zx}	Q_x						\checkmark	\checkmark
AFO	M_{xyz}	M_{xy}						\checkmark	
AFO	M_z^β	M_v		\checkmark				\checkmark	\checkmark

the ordered state do not couple with $Q_u^{(c)}$ or $M_z^{(c)}$. Meanwhile, each frequency is shifted by $[Q_z^{(c)}]^{4/3}$, which is understood by the behavior of $Q_u^{(c)}$, as discussed in Sec. IV B.

For fully saturated $Q_z^{(c)} = 0.5$, all the NMR frequencies become $f \sim 5.2$, which corresponds to the frequency only in the external magnetic field. This is because $Q_u^{(c)}$ in the crystal-field term vanishes for $Q_z^{(c)} = 0.5$, as shown in Fig. 2(h).

4. Staggered M_x -type AFM

In the M_x -type AFM state, the effective nuclear Hamiltonian for the Co nucleus is represented as

$$\mathcal{H}_{\text{CoA(B)}} = (-H_z^{(n)} + c'M_z^{(c)})\hat{I}_z \pm c'T_y^{(c)}\hat{I}_x + c_Q Q_u^{(c)}\hat{I}_u + cQ_v^{(c)}\hat{I}_v, \quad (38)$$

$$\tilde{\mathcal{H}}_{\text{CoA(B)}} = c'Q_u^{(c)}\hat{I}_z + c'M_z^{(c)}\hat{I}_u \pm c'T_y^{(c)}\hat{I}_{zx}. \quad (39)$$

The NMR spectra for $c = 0.3$ and $c' = 0.02$ are shown in Fig. 4(c). The spectra show no sublattice-dependent splitting, which is similar to those in the NQR spectra in Sec. IV C, as $T_y^{(c)}$ does not couple with $Q_u^{(c)}$ or $M_z^{(c)}$. The shift of the resonance frequency in relation to $T_y^{(c)}$ is small compared to that in the Q_u -type AFQ state in Fig. 4(b), which reflects the different behavior of $Q_u^{(c)}$, as shown in Fig. 2(i).

B. The [100]-field spectrum

We show the [100]-field NMR spectrum in the paramagnetic state, Q_v -type AFQ state, Q_u -type AFQ state, and M_x -type AFM state in Secs. VB 1–VB 4, respectively.

1. Paramagnetic state

In the paramagnetic state in the [100] magnetic field, the effective nuclear Hamiltonian of the Co nucleus is represented by

$$\mathcal{H}_{\text{CoA(B)}} = (-H_x^{(n)} + c'M_x^{(c)})\hat{I}_x + c_Q Q_u^{(c)}\hat{I}_u + c'Q_v^{(c)}\hat{I}_v. \quad (40)$$

$$\tilde{\mathcal{H}}_{\text{CoA(B)}} = c'(Q_u^{(c)} + Q_v^{(c)})\hat{I}_x + c'(Q_v^{(c)} + M_x^{(c)})\hat{I}_u + c'(Q_u^{(c)} + M_x^{(c)})\hat{I}_v. \quad (41)$$

The nuclear Hamiltonian in Eqs. (40) and (41) leads to seven spectra similar to those in the [001] magnetic field. However, the intervals between the resonance frequencies are not equivalent, since the magnetic field normal to the z axis leads to the emergence of $Q_v^{(c)}$.

2. Staggered Q_v -type AFQ

In the Q_v -type AFQ state, the effective nuclear Hamiltonian is described as

$$\mathcal{H}_{\text{CoA(B)}} = (-H_x^{(n)} + c'M_x^{(c)})\hat{I}_x + (c_Q Q_u^{(c)} \pm cG_{xy}^{(c)})\hat{I}_u + c'Q_v^{(c)}\hat{I}_v, \quad (42)$$

$$\begin{aligned} \tilde{\mathcal{H}}_{\text{CoA(B)}} &= [c'(Q_u^{(c)} + Q_v^{(c)} \pm Q_z^{(c)} \pm G_{xy}^{(c)}) \pm c'_M T_y^{(c)}]\hat{I}_x \\ &+ c'(Q_v^{(c)} + M_x^{(c)} \pm Q_z^{(c)} \pm T_y^{(c)})\hat{I}_u \\ &+ c'(Q_u^{(c)} + M_x^{(c)} \pm Q_z^{(c)} \pm G_{xy}^{(c)} \pm T_y^{(c)})\hat{I}_v. \end{aligned} \quad (43)$$

Figure 4(d) shows the [100]-field NMR spectra for $c = c' = 0.02$ and $c'_M = 0.3$, where the color scale represents the intensity of the NMR spectra. The result indicates that sublattice-dependent spectral splitting occurs as well as the results for NQR (Sec. IV A) and [001]-field NMR (Sec. VA 2). Also in the [100]-field NMR, the spectrum is mainly determined by the following dominant contributions: the Zeeman term, the $c_Q Q_u^{(c)}$ term, and primarily induced $G_{xy}^{(c)}$ terms. In other words, among the odd-parity multipoles $G_{xy}^{(c)}$, $Q_z^{(c)}$, and $T_y^{(c)}$, the important contribution comes from $G_{xy}^{(c)}$, since the magnitudes of $Q_z^{(c)}$ and $T_y^{(c)}$ are much smaller than that of $G_{xy}^{(c)}$, as shown in Fig. 2(j). Meanwhile, the shift of the spectra is dominated by $Q_u^{(c)}$.

3. Staggered Q_u -type AFQ

The effective nuclear Hamiltonian in the Q_u -type AFQ state is

$$\mathcal{H}_{\text{CoA(B)}} = (-H_x^{(n)} + c'M_x^{(c)})\hat{I}_x + c_Q Q_u^{(c)}\hat{I}_u + (c'Q_v^{(c)} \pm cQ_z^{(c)})\hat{I}_v, \quad (44)$$

$$\begin{aligned} \tilde{H}_{\text{Co}_{\text{A(B)}}} = & [c'(Q_u^{(c)} + Q_v^{(c)} \pm Q_z^{(c)} \pm G_{xy}^{(c)}) \pm c'_M T_y^{(c)}] \hat{I}_x \\ & + c'(Q_v^{(c)} + M_x^{(c)} \pm G_{xy}^{(c)} \pm Q_z^{(c)} \pm T_y^{(c)}) \hat{I}_u \\ & + c'(Q_u^{(c)} + M_x^{(c)} \pm G_{xy}^{(c)} \pm T_y^{(c)}) \hat{I}_v, \end{aligned} \quad (45)$$

which is the same as that in the Q_v -type AFQ state in Eqs. (42) and (43), as the magnetic point group symmetry in the magnetic field is the same as $2'mm'$ in this case. Thus, in contrast to the results for the NQR (Sec. IV B) and [001]-field NMR (Sec. V A 3), the sublattice-dependent splittings occur in the [100] magnetic field as shown in the NMR spectra for $c = c' = 0.02$ and $c'_M = 0.3$ in Fig. 4(e).

However, the mean-field dependence of the spectra is different from that in the Q_v -type AFQ state, since the magnitude of $Q_z^{(c)}$ is much larger than that of other multipoles. In particular, the spectral shift reflects the different mean-field dependence of $Q_u^{(c)}$, as already discussed in Sec. IV B.

4. Staggered M_x -type AFM

The nuclear Hamiltonian in the M_x -type AFM state is

$$H_{\text{Co}_{\text{A(B)}}} = (-H_x^{(n)} + c'M_x^{(c)} \pm cT_y^{(c)}) \hat{I}_x + c_Q Q_u^{(c)} \hat{I}_u + c'Q_v^{(c)} \hat{I}_v, \quad (46)$$

$$\begin{aligned} \tilde{H}_{\text{Co}_{\text{A(B)}}} = & c'(Q_u^{(c)} + Q_v^{(c)} \pm Q_z^{(c)} \pm G_{xy}^{(c)}) \hat{I}_x \\ & + c'(Q_v^{(c)} + M_x^{(c)} \pm G_{xy}^{(c)} \pm Q_z^{(c)} \pm T_y^{(c)}) \hat{I}_u \\ & + c'(Q_u^{(c)} + M_x^{(c)} \pm G_{xy}^{(c)} \pm Q_z^{(c)} \pm T_y^{(c)}) \hat{I}_v, \end{aligned} \quad (47)$$

where the same multipoles appear in the two AFQ states in Eqs. (42)–(45), since the magnetic point group symmetry in the [100] magnetic field reduces to $2'mm'$ also in this case. Thus, the sublattice-dependent NMR splittings occur, which are similar to those in the AFQ states. However, the dominant odd-parity multipole to induce the spectral splitting is given by $T_y^{(c)}$. The [100]-field NMR spectra for $c = 0.3$ and $c' = 0.02$ is shown in Fig. 4(f).

VI. SPECTRAL SPLITTINGS FOR ODD-PARITY MULTIPOLES

So far, we have focused on the NQR and NMR spectra in the two AFQ and AFM ordered states in the magnetic fields along the [001] and [100] directions as well as the zero magnetic field. In a similar way, possible NQR and NMR splittings in other odd-parity multipole orderings in any field directions can be calculated. We show the presence or absence of the sublattice-dependent NQR and NMR splittings for the other candidate odd-parity multipole orders in CeCoSi, which are expected from the low-energy crystal-field level. The present analysis is applicable once the phase transition occurs in the magnetic field unless the second-excited levels are involved in the phase transition. It should be noted that our analysis can be extended to other electronic orderings in different crystal-field levels as discussed in Appendix D and other multiorbital systems.

The results in the present Γ_6 - Γ_7 levels are summarized in Table V. We list the other candidates, as discussed in Sec. II A: two AFM states, three AFQ states, and two antiferromagnetic octupole (AFO) states. We also include

the results in the Q_v - and Q_u -type AFQ states and the M_x -type AFM state discussed in Secs. IV and V in the other magnetic-field directions. The table exhibits when the sublattice-dependent spectral splittings occur in the presence of odd-parity multipoles. For example, in the AFQ phase, the NMR measurement in the zx -plane (yz -plane) magnetic field is useful in identifying the odd-parity multipole order parameter; the sublattice-dependent splittings which always appear when the magnetic-field direction is rotated in the zx (yz) plane indicate the emergence of $G_{xy}^{(c)}$. Meanwhile, in the AFM phase, the sublattice-dependent splittings in the magnetic field along the x direction will indicate the presence of $T_y^{(c)}$. In this way, as the different spectral splittings are found in the different odd-parity multipole orderings depending on the magnetic-field directions, the detailed investigation of the field angle dependence enables us to identify the order parameter in CeCoSi.

VII. SUMMARY

We have discussed the effect of the odd-parity multipoles on the NQR and NMR spectra. First, we derived the hyperfine field of the Co nuclei in consideration of the contribution from the electronic multipole moments at Ce sites. We showed that the hyperfine field in the presence of the odd-parity multipole moments causes the sublattice-dependent splittings of the NQR and NMR spectra. Moreover, we obtained the different spectral splittings for the different odd-parity multipoles by considering the NQR spectral splitting as well as [001]- and [100]-field NMR spectral splittings in the three ordered states: the M_x -type AFM state with $T_y^{(c)}$ and Q_v - and Q_u -type AFQ states with $G_{xy}^{(c)}$ and $Q_z^{(c)}$, respectively.

We emphasize that not only the even-parity multipoles but also the odd-parity multipoles affect the nuclear spin unless the NMR site is located at the inversion center. As the key ingredient is the emergence of the cluster odd-parity multipoles, which consist of the spatial distributions of the even-parity multipoles such as magnetic dipoles and electric quadrupoles, the odd-parity-hosting candidate materials to have the AFM structures, e.g., Ce_3TlBi_5 [76] and AOsO_4 ($A = \text{K, Rb, Cs}$) [77], might be good targeting materials.

ACKNOWLEDGMENTS

We thank M. Manago, K. Kotegawa, H. Tou, H. Tanida, and Y. Ihara for the fruitful discussions on experimental information on CeCoSi. This research was supported by JSPS KAKENHI Grants No. JP18K13488, No. JP19K03752, and No. JP19H01834 and JST PREST (JPMJPR20L8). M.Y. was supported by a JSPS research fellowship and by JSPS KAKENHI Grant No. JP20J12026.

APPENDIX A: MULTIPOLE MOMENTS IN CONJUGATE MEAN FIELDS

In this Appendix we discuss the different mean-field dependences of $G_{xy}^{(c)}$ in the Q_v -type AFQ state and $Q_z^{(c)}$ in the Q_u -type AFQ state from Sec. II C. The result from the numerical diagonalization indicates that $G_{xy}^{(c)}$ roughly increases as a

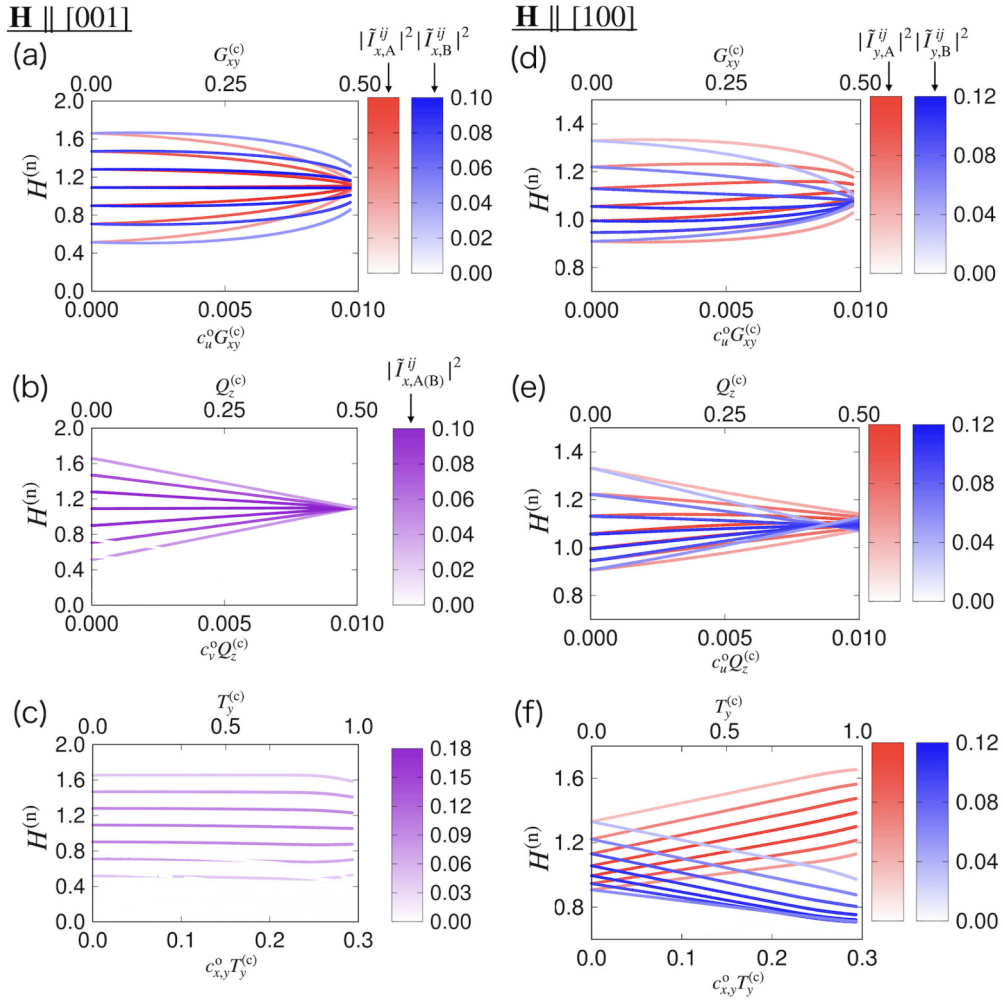


FIG. 5. Odd-parity multipole dependences of the field-swept NMR spectra in the (a)–(c) [001] magnetic field and (d)–(f) [100] magnetic field. The data are for the (a) and (d) Q_v -type AFQ, (b) and (e) Q_u -type AFQ, and (c) and (f) M_x -type AFM states. The color scales represent the intensities with (a)–(c) $|\tilde{I}_{x,A}^{ij}|^2$ and (d)–(f) $|\tilde{I}_{y,A}^{ij}|^2$. The coupling constants are $c_u^o = c_v^o = c = 0.02$ in the AFQ states and $c_{x,y}^o = c = 0.3$ in the AFM state. Other coupling constants are set to be $c' = 0.02$.

function of $h_{Q_v}^s$, whereas $Q_z^{(c)}$ increases as a function of $(h_{Q_u}^s)^3$ in the small h_X^s region as shown in Figs. 2(d) and 2(e).

The difference is understood by the power expansion of the multipole moments

$$\tilde{X}^{(c)} = X_A - X_B = a_X^{(1)}(h_X^s) + a_X^{(3)}(h_X^s)^3 + \dots, \quad (\text{A1})$$

where $\tilde{X}^{(c)} = G_{xy}^{(c)}(Q_z^{(c)})$ for $X = Q_v(Q_u)$ and $a_X^{(n)}$ are the coefficients that depend on the crystal-field splitting Δ . It should be noted that the even order of h_X^s does not appear due to the different parity with respect to the inversion symmetry.

For large Δ , by treating the mean-field term in Eq. (1) perturbatively, the basis function at the Ce_i site in the Q_v -type AFQ state changes into

$$\tilde{\phi}_{\Gamma_7\sigma,i} = \frac{1}{N} \left(\phi_{\Gamma_7\sigma,i} \pm \frac{h_{Q_v}^s}{2\Delta} \phi_{\Gamma_6\sigma,i} \right), \quad (\text{A2})$$

where the sign $+$ ($-$) is taken for $i = A$ (B), N is the normalization factor, and $\sigma = \uparrow, \downarrow$ is the quasispin. Then $G_{xy}^{(c)}$ is

obtained as

$$G_{xy}^{(c)} = \frac{1}{N} \frac{h_{Q_v}^s}{2\Delta} = \left[1 + \left(\frac{h_{Q_v}^s}{2\Delta} \right)^2 \right]^{-1/2} \frac{h_{Q_v}^s}{2\Delta} \\ \sim \frac{1}{2\Delta} h_{Q_v}^s - \left(\frac{1}{2\Delta} \right)^3 (h_{Q_v}^s)^3. \quad (\text{A3})$$

This indicates that $a_{Q_v}^{(1)} (= \frac{1}{2\Delta}) \gg a_{Q_v}^{(3)} [= (\frac{1}{2\Delta})^3]$ is satisfied for $h_{Q_v}^s/\Delta \ll 1$, which results in the linear behavior of $G_{xy}^{(c)}$ in Fig. 2(d). In a similar way, the linear behavior of $T_y^{(c)}$ in Fig. 2(f) is accounted for in the M_x -type AFM state.

In contrast, in the Q_u -type AFQ state, $Q_z^{(c)}$ becomes zero for large Δ , which means that

$$Q_z^{(c)} = 0 \quad (\Delta > h_{Q_u}^s), \quad (\text{A4})$$

$$Q_z^{(c)} = 1 \quad (\Delta < h_{Q_u}^s). \quad (\text{A5})$$

Thus, the onset of $Q_z^{(c)}$ for small $h_{Q_u}^s$ in Fig. 2(e) is due to the finite-temperature effect. Numerically, the opposite relation ($a_{Q_u}^{(1)} \ll a_{Q_u}^{(3)}$) to the Q_u -type AFQ ordered case with respect

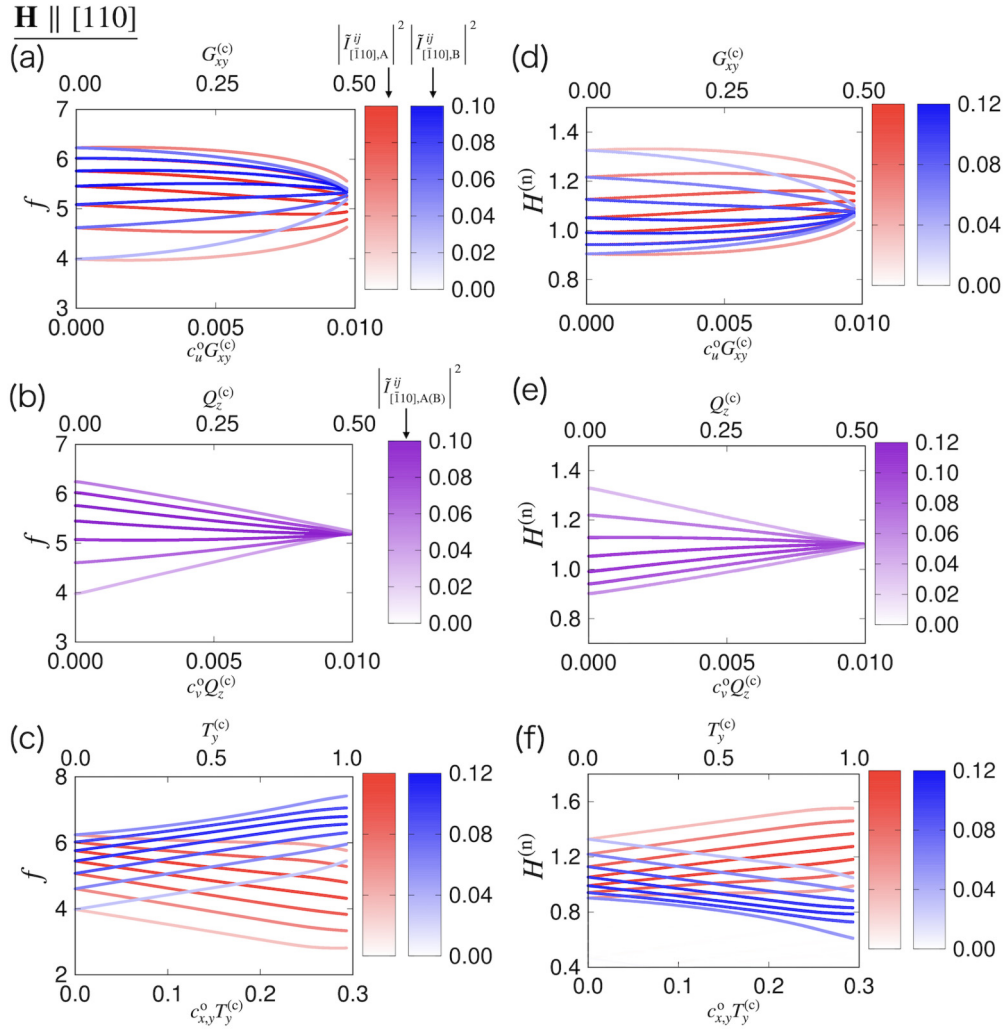


FIG. 6. Odd-parity multipole dependences of the (a)–(c) frequency-swept NMR spectra and (d)–(f) field-swept NMR spectra in the [110] magnetic field. The data are for the (a) and (d) Q_v -type AFQ, (b) and (e) Q_u -type AFQ, and (c) and (f) M_x -type AFM states. The color scales represent the intensities with $|\tilde{I}_{[110],A(B)}^{ij}|^2$. The coupling constants are $c_u^o = c_v^o = 0.02$ in the AFQ states and $c_{x,y}^o = 0.3$ in the AFM state. Other coupling constants are set to be $c' = 0.02$.

to $a_{Q_u}^{(1)}$ and $a_{Q_u}^{(3)}$ is obtained for large Δ ; $a_{Q_u}^{(1)} \sim 10^{-2} a_{Q_u}^{(3)}$ for $\Delta = 0.5$ and $\beta = 10$. This implies that $Q_z^{(c)}$ increases as a function of $(h_{Q_u}^s)^3$ in the small $h_{Q_u}^s$ region in Fig. 2(e).

APPENDIX B: FIELD-SWEPT NMR

We show the field-swept NMR spectra for the resonance frequency $\omega = 1.1\gamma$ in the [001] and [100] magnetic

fields. We set $\gamma = 1$ and the coupling constant as well as that in Sec. V. Figures 5(a)–5(c) show the spectra in the [001] magnetic field, whereas Figs. 5(d)–5(f) show those in the [100] magnetic field. The results show a similar tendency in the cases of the frequency-swept spectra in Fig. 4.

APPENDIX C: THE [110]-FIELD NMR

We show the effective hyperfine fields and NMR spectra in the case of the [110] magnetic field in the Q_v - and Q_u -type AFQ states and the M_x -type AFM state. The hyperfine field Hamiltonian is given by

$$\begin{aligned} \tilde{\mathcal{H}}_{\text{para}}^{[110]} &= (\tilde{c}_{x,y}^{e,1} Q_u^{(c)} + \tilde{c}_{x,y}^{e,2} Q_{xy}^{(c)}) (\hat{I}_x + \hat{I}_y) + [\tilde{c}_u^{e,1} Q_{xy}^{(c)} + \tilde{c}_u^{e,2} (M_x^{(c)} + M_y^{(c)})] \hat{I}_u + [\tilde{c}_{xy}^{e,1} Q_u^{(c)} + \tilde{c}_{xy}^{e,2} (M_x^{(c)} + M_y^{(c)})] \hat{I}_{xy}, \\ \tilde{\mathcal{H}}_{\text{order}}^{[110]} &= \tilde{c}_{x,y}^{o,1} G_{xy}^{(c)} (\hat{I}_x + \hat{I}_y) + [\tilde{c}_{x,y}^{o,2} (T_x^{(c)} - T_y^{(c)}) + \tilde{c}_{x,y}^{o,3} Q_z^{(c)} + \tilde{c}_{x,y}^{o,4} G_u^{(c)}] (\hat{I}_x - \hat{I}_y) + \tilde{c}_z^o (Q_x^{(c)} - Q_y^{(c)}) \hat{I}_z \\ &\quad + \tilde{c}_u^o (T_x^{(c)} + T_y^{(c)}) \hat{I}_u + [\tilde{c}_v^{o,1} G_v^{(c)} + \tilde{c}_v^{o,2} (T_x^{(c)} - T_y^{(c)})] \hat{I}_v + [\tilde{c}_{yz,zx}^{o,1} M_u^{(c)} + \tilde{c}_{yz,zx}^{o,2} M_{xy}^{(c)}] (\hat{I}_{yz} - \hat{I}_{zx}) \end{aligned} \quad (\text{C1})$$

TABLE VI. Sublattice-dependent NQR and NMR splittings in the AFM, AFQ, AFH, and AFT states in the six field directions [001], [100], [110], \perp [001], \perp [010], and \perp [$\bar{1}10$], when the crystal-field first-excited state is a Γ_7 doublet. The local multipoles (LMP) at the Ce site and cluster odd-parity multipoles (OPMP) are shown in the second and third columns, respectively. The mark \checkmark represents the presence of the sublattice-dependent splittings.

State	LMP	OPMP	NQR	NMR					
				$\mathbf{H}_{\parallel[001]}$	$\mathbf{H}_{\parallel[100]}$	$\mathbf{H}_{\parallel[110]}$	$\mathbf{H}_{\perp[001]}$	$\mathbf{H}_{\perp[010]}$	$\mathbf{H}_{\perp[\bar{1}10]}$
AFM	M_x	T_y			\checkmark	\checkmark	\checkmark	\checkmark	\checkmark
AFM	M_y	T_x				\checkmark	\checkmark		\checkmark
AFM	M_z	M_u						\checkmark	
AFQ	Q_u	Q_z		\checkmark			\checkmark	\checkmark	
AFQ	Q_{yz}	Q_y							\checkmark
AFQ	Q_{zx}	Q_x						\checkmark	\checkmark
AFH	Q_{4z}^α	G_u				\checkmark	\checkmark		\checkmark
AFT	M_{5u}	T_z							\checkmark

$$+ [\tilde{c}_{yz,zx}^{0,3} (Q_x^{(c)} - Q_y^{(c)}) + \tilde{c}_{yz,zx}^{0,4} M_v^{(c)}] (\hat{I}_{yz} + \hat{I}_{zx}) + [\tilde{c}_{xy}^{0,1} G_{xy}^{(c)} + \tilde{c}_{xy}^{0,2} (T_x^{(c)} + T_y^{(c)})] \hat{I}_{xy}, \quad (\text{C2})$$

$$\begin{aligned} \tilde{\mathcal{H}}_{\text{order}}^{\text{el}[110]} = & [\tilde{c}_{x,y}^{e,3} (M_x^{(c)} - M_y^{(c)}) + \tilde{c}_{x,y}^{e,4} Q_v^{(c)}] (\hat{I}_x - \hat{I}_y) + [\tilde{c}_z^{e,1} (Q_{yz}^{(c)} + Q_{zx}^{(c)}) + \tilde{c}_z^{e,2} M_{xyz}^{(c)}] \hat{I}_z \\ & + \tilde{c}_v^e (M_x^{(c)} - M_y^{(c)}) \hat{I}_v + \tilde{c}_{yz,zx}^{e,1} M_z^{\beta(c)} (\hat{I}_{yz} - \hat{I}_{zx}) + [\tilde{c}_{yz,zx}^{e,2} (Q_{yz}^{(c)} + Q_{zx}^{(c)}) + \tilde{c}_{yz,zx}^{e,3} M_z^{(c)} + \tilde{c}_{yz,zx}^{e,4} M_{xyz}^{(c)}] (\hat{I}_{yz} + \hat{I}_{zx}). \end{aligned} \quad (\text{C3})$$

We set the coupling constants as $c_u^e = c_Q = 0.13$ and $c_{x,y}^o = 0.3$ and the others are set to be 0.02 for simplicity.

Figures 6(a)–6(c) show the frequency-swept NMR spectra for the magnetic field $|\mathbf{H}^{(n)}| = 1$, whereas Figs. 6(d)–6(f) are the field-swept NMR spectra for the resonance frequency $\omega = 1.1\gamma$, where γ is set to be 1. The intensity of the spectra is calculated as $|\tilde{I}_{[110],A(B)}^{ij}|^2$ for $I_{[110]} = (I_x - I_y)/2$.

In the Q_v -type AFQ [Figs. 6(a) and 6(d)] and M_x -type AFM states [Figs. 6(d) and 6(f)], the splittings in the [110] field show a similar tendency to those in the [100] field in Secs. VB 2 and VB 4. Their splittings are dominantly characterized by $G_{xy}^{(c)}$ and $T_y^{(c)}$, respectively. On the other hand, in the Q_u -type AFQ state in Figs. 6(b) and 6(e), there are no spectral splittings, in contrast to the result in the [100] field in Sec. VB 3. The reason why no splittings occur in the [110] field is attributed to the difference of the site symmetry at the Co site. As the present site symmetry is $2'22'$, which is different from $2'mm'$ in the [100] direction, there is no coupling between odd-parity $Q_z^{(c)}$ and any of $I_x + I_y$, I_u , and I_{xy} in Eq. (C2).

APPENDIX D: SPECTRAL SPLITTINGS FOR OTHER LOW-ENERGY CRYSTAL-FIELD LEVELS

The different low-energy crystal-field levels activate different types of odd-parity multipole orderings. In this Appendix we show the expected sublattice-dependent splittings in NQR and NMR spectra by supposing the low-energy crystal-field level consists of the two Γ_7 doublets [56]. In this case, two other multipole orderings become possible: Q_{4z}^α -type antiferroic hexadecapole ordering (AFH) with the odd-parity electric toroidal quadrupole G_u and M_{5u} -type antiferroic tria-

contadipole ordering (AFT) with the magnetic toroidal dipole T_z . The functional forms of Q_{4z}^α and M_{5u} are shown in Ref. [78].

By performing a procedure similar to that in Secs. III–V, the presence or absence of the sublattice-dependent spectral splittings in NQR and NMR is obtained. The results are summarized in Table VI. The common multipoles appearing in both the two Γ_7 doublets and Γ_6 - Γ_7 doublets, T_x , T_y , M_u , Q_z , Q_x , and Q_y , give the same result in Table V. Note that electric toroidal quadrupoles G_v and G_{xy} and magnetic quadrupoles M_v and M_{xy} are not activated within the low-energy crystal-field levels unless the first-excited state is a Γ_6 doublet.

- [1] M. Fiebig, *J. Phys. D* **38**, R123 (2005).
- [2] J. van den Brink and D. I. Khomskii, *J. Phys.: Condens. Matter* **20**, 434217 (2008).
- [3] Y. Tokura, S. Seki, and N. Nagaosa, *Rep. Prog. Phys.* **77**, 076501 (2014).
- [4] Y. Tokura and N. Nagaosa, *Nat. Commun.* **9**, 3740 (2018).

- [5] N. A. Spaldin, M. Fiebig, and M. Mostovoy, *J. Phys.: Condens. Matter* **20**, 434203 (2008).
- [6] S. Hayami, H. Kusunose, and Y. Motome, *Phys. Rev. B* **90**, 024432 (2014).
- [7] S. Hayami, H. Kusunose, and Y. Motome, *J. Phys. Soc. Jpn.* **84**, 064717 (2015).

- [8] H. Saito, K. Uenishi, N. Miura, C. Tabata, H. Hidaka, T. Yanagisawa, and H. Amitsuka, *J. Phys. Soc. Jpn.* **87**, 033702 (2018).
- [9] F. Thöle and N. A. Spaldin, *Philos. Trans. R. Soc. A* **376**, 20170450 (2018).
- [10] N. D. Khanh, N. Abe, S. Kimura, Y. Tokunaga, and T. Arima, *Phys. Rev. B* **96**, 094434 (2017).
- [11] Y. Yanagi, S. Hayami, and H. Kusunose, *Phys. Rev. B* **97**, 020404(R) (2018).
- [12] H. Watanabe and Y. Yanase, *Phys. Rev. B* **96**, 064432 (2017).
- [13] L. Fu, *Phys. Rev. Lett.* **115**, 026401 (2015).
- [14] S. Hayami, Y. Yanagi, H. Kusunose, and Y. Motome, *Phys. Rev. Lett.* **122**, 147602 (2019).
- [15] T. Hitomi and Y. Yanase, *J. Phys. Soc. Jpn.* **83**, 114704 (2014).
- [16] T. Hitomi and Y. Yanase, *J. Phys. Soc. Jpn.* **85**, 124702 (2016).
- [17] T. Hitomi and Y. Yanase, *J. Phys. Soc. Jpn.* **88**, 054712 (2019).
- [18] Y. Yanase, *J. Phys. Soc. Jpn.* **83**, 014703 (2014).
- [19] S. Hayami, H. Kusunose, and Y. Motome, *Phys. Rev. B* **97**, 024414 (2018).
- [20] T. Ishitobi and K. Hattori, *J. Phys. Soc. Jpn.* **88**, 063708 (2019).
- [21] B. B. Van Aken, J.-P. Rivera, H. Schmid, and M. Fiebig, *Nature (London)* **449**, 702 (2007).
- [22] A. S. Zimmermann, D. Meier, and M. Fiebig, *Nat. Commun.* **5**, 4796 (2014).
- [23] L. Alagna, T. Prosperi, S. Turchini, J. Goulon, A. Rogalev, C. Goulon-Ginet, C. R. Natoli, R. D. Peacock, and B. Stewart, *Phys. Rev. Lett.* **80**, 4799 (1998).
- [24] J. Goulon, C. Goulon-Ginet, A. Rogalev, V. Gotte, C. Malgrange, C. Brouder, and C. R. Natoli, *J. Chem. Phys.* **108**, 6394 (1998).
- [25] J. Goulon, C. Goulon-Ginet, A. Rogalev, V. Gotte, C. Malgrange, and C. Brouder, *J. Synchrotron Radiat* **6**, 673 (1999).
- [26] J. Goulon, C. Goulon-Ginet, A. Rogalev, G. Benayoun, C. Brouder, and C. R. Natoli, *J. Synchrotron Radiat* **7**, 182 (2000).
- [27] J. Goulon, A. Rogalev, C. Goulon-Ginet, G. Benayoun, L. Paolasini, C. Brouder, C. Malgrange, and P. A. Metcalf, *Phys. Rev. Lett.* **85**, 4385 (2000).
- [28] J. Goulon, A. Rogalev, F. Wilhelm, C. Goulon-Ginet, P. Carra, D. Cabaret, and C. Brouder, *Phys. Rev. Lett.* **88**, 237401 (2002).
- [29] M. Kubota, T. Arima, Y. Kaneko, J. P. He, X. Z. Yu, and Y. Tokura, *Phys. Rev. Lett.* **92**, 137401 (2004).
- [30] T.-h. Arima, J.-H. Jung, M. Matsubara, M. Kubota, J.-P. He, Y. Kaneko, and Y. Tokura, *J. Phys. Soc. Jpn.* **74**, 1419 (2005).
- [31] K. Kimura, T. Katsuyoshi, Y. Sawada, S. Kimura, and T. Kimura, *Commun. Mater.* **1**, 39 (2020).
- [32] M. Kawakami, S. Kunii, K. Mizuno, M. Sugita, T. Kasuya, and K. Kume, *J. Phys. Soc. Jpn.* **50**, 432 (1981).
- [33] M. Kawakami, K. Mizuno, S. Kunii, T. Kasuya, H. Enokiya, and K. Kume, *J. Magn. Magn. Mater.* **30**, 201 (1982).
- [34] M. Kawakami, H. Bohn, H. Lütgemeier, S. Kunii, and T. Kasuya, *J. Magn. Magn. Mater.* **31**, 415 (1983).
- [35] M. Takigawa, H. Yasuoka, T. Tanaka, and Y. Ishizawa, *J. Phys. Soc. Jpn.* **52**, 728 (1983).
- [36] O. Sakai, R. Shiina, H. Shiba, and P. Thalmeier, *J. Phys. Soc. Jpn.* **66**, 3005 (1997).
- [37] R. Shiina, O. Sakai, H. Shiba, and P. Thalmeier, *J. Phys. Soc. Jpn.* **67**, 941 (1998).
- [38] O. Sakai, R. Shiina, H. Shiba, and P. Thalmeier, *J. Phys. Soc. Jpn.* **68**, 1364 (1999).
- [39] K. Hanzawa, *J. Phys. Soc. Jpn.* **68**, 1063 (1999).
- [40] K. Hanzawa, *J. Phys. Soc. Jpn.* **69**, 510 (2000).
- [41] S. Tsuji, M. Sera, and K. Kojima, *J. Phys. Soc. Jpn.* **70**, 41 (2001).
- [42] S. Tsuji, M. Sera, and K. Kojima, *J. Phys. Soc. Jpn.* **70**, 2864 (2001).
- [43] K. Magishi, M. Kawakami, T. Saito, K. Koyama, K. Mizuno, and S. Kunii, *Z. Naturforsch. A* **57**, 441 (2002).
- [44] O. Sakai, R. Shiina, and H. Shiba, *J. Phys. Soc. Jpn.* **74**, 457 (2005).
- [45] Y. Tokunaga, Y. Homma, S. Kambe, D. Aoki, H. Sakai, E. Yamamoto, A. Nakamura, Y. Shiokawa, R. E. Walstedt, and H. Yasuoka, *Phys. Rev. Lett.* **94**, 137209 (2005).
- [46] Y. Tokunaga, D. Aoki, Y. Homma, S. Kambe, H. Sakai, S. Ikeda, T. Fujimoto, R. E. Walstedt, H. Yasuoka, E. Yamamoto, A. Nakamura, and Y. Shiokawa, *Phys. Rev. Lett.* **97**, 257601 (2006).
- [47] K. Ishida, H. Murakawa, K. Kitagawa, Y. Ihara, H. Kotegawa, M. Yogi, Y. Kitaoka, B.-L. Young, M. S. Rose, D. E. MacLaughlin, H. Sugawara, T. D. Matsuda, Y. Aoki, H. Sato, and H. Harima, *Phys. Rev. B* **71**, 024424 (2005).
- [48] J. Kikuchi, M. Takigawa, H. Sugawara, and H. Sato, *Physica B* **359**, 877 (2005).
- [49] O. Sakai, J. Kikuchi, R. Shiina, H. Sato, H. Sugawara, M. Takigawa, and H. Shiba, *J. Phys. Soc. Jpn.* **76**, 024710 (2007).
- [50] J. Kikuchi, M. Takigawa, H. Sugawara, and H. Sato, *J. Phys. Soc. Jpn.* **76**, 043705 (2007).
- [51] B. Chevalier, S. F. Matar, J. S. Marcos, and J. R. Fernandez, *Physica B* **378**, 795 (2006).
- [52] E. Lengyel, M. Nicklas, N. Caroca-Canales, and C. Geibel, *Phys. Rev. B* **88**, 155137 (2013).
- [53] H. Tanida, Y. Muro, and T. Matsumura, *J. Phys. Soc. Jpn.* **87**, 023705 (2018).
- [54] H. Tanida, K. Mitsumoto, Y. Muro, T. Fukuhara, Y. Kawamura, A. Kondo, K. Kindo, Y. Matsumoto, T. Namiki, T. Kuwai, and T. Matsumura, *J. Phys. Soc. Jpn.* **88**, 054716 (2019).
- [55] Y. Kawamura, H. Tanida, R. Ueda, J. Hayashi, K. Takeda, and C. Sekine, *J. Phys. Soc. Jpn.* **89**, 054702 (2020).
- [56] S. E. Nikitin, D. G. Franco, J. Kwon, R. Bewley, A. Podlesnyak, A. Hoser, M. M. Koza, C. Geibel, and O. Stockert, *Phys. Rev. B* **101**, 214426 (2020).
- [57] H. Tanida, K. Mitsumoto, Y. Muro, T. Fukuhara, Y. Kawamura, A. Kondo, K. Kindo, Y. Matsumoto, T. Namiki, T. Kuwai, and T. Matsumura, *JPS Conf. Proc.* **30**, 011156 (2020).
- [58] S. Chandra, A. Khatun, and R. Jannat, *Solid State Commun* **316–317**, 113953 (2020).
- [59] O. Bodak, E. Gladyshevskii, and P. Kripyakevich, *J. Struct. Chem* **11**, 283 (1970).
- [60] M. Yatsushiro and S. Hayami, *J. Phys. Soc. Jpn.* **89**, 013703 (2020).
- [61] M. Yatsushiro and S. Hayami, *JPS Conf. Proc.* **30**, 011151 (2020).
- [62] H. Kusunose, *J. Phys. Soc. Jpn.* **77**, 064710 (2008).
- [63] Y. Kuramoto, H. Kusunose, and A. Kiss, *J. Phys. Soc. Jpn.* **78**, 072001 (2009).
- [64] P. Santini, S. Carretta, G. Amoretti, R. Caciuffo, N. Magnani, and G. H. Lander, *Rev. Mod. Phys.* **81**, 807 (2009).

- [65] M.-T. Suzuki, H. Ikeda, and P. M. Oppeneer, *J. Phys. Soc. Jpn.* **87**, 041008 (2018).
- [66] F. J. Ohkawa, *J. Phys. Soc. Jpn.* **54**, 3909 (1985).
- [67] S. Hayami and H. Kusunose, *J. Phys. Soc. Jpn.* **87**, 033709 (2018).
- [68] H. Kusunose, R. Oiwa, and S. Hayami, *J. Phys. Soc. Jpn.* **89**, 104704 (2020).
- [69] There are two other magnetic multipole degrees of freedom consisting of the x or y component of one interorbital and two intraorbital magnetic dipoles, which are orthogonal to each other. For the z component, there is another magnetic multipole degree of freedom from two intraorbital magnetic dipoles.
- [70] In addition to the magnetic dipole case, there is another electric multipole degree of freedom from $\hat{Q}_0^{(c)}$ and $\hat{Q}_u^{(c)}$ in the same irreducible representation with $\hat{Q}_z^{(c)}$.
- [71] We also avoid the situation where some multipole moments, such as Q_{yz} , Q_{zx} , Q_{xy} , M_{xyz} , T_x , T_y , M_u , and M_{xy} , vanish by taking specific values $\delta^{\Gamma_6} = \delta' = 1$ in the Q_u -type AFQ state for the magnetic field in the plane normal to the $[\bar{1}10]$ direction.
- [72] T. Das and E. Hahn, *Solid State Physics Supplement* (Academic, New York, 1958), Vol. 1.
- [73] The following result does not change for nonzero C_v^{CF} in the present model.
- [74] A. P. Cracknell, *Prog. Theor. Phys.* **35**, 196 (1966).
- [75] M. Manago, K. Kotegawa, H. Tou, and H. Tanida, J-Physics Annual Meeting FY2019, Kobe, 2020 (unpublished), P05.
- [76] M. Shinozaki, G. Motoyama, M. Tsubouchi, M. Sezaki, J. Gouchi, S. Nishigori, T. Mutou, A. Yamaguchi, K. Fujiwara, K. Miyoshi, and Y. Uwatoko, *J. Phys. Soc. Jpn.* **89**, 033703 (2020).
- [77] J.-i. Yamaura and Z. Hiroi, *Phys. Rev. B* **99**, 155113 (2019).
- [78] S. Hayami, M. Yatsushiro, Y. Yanagi, and H. Kusunose, *Phys. Rev. B* **98**, 165110 (2018).